Electric Discharge Initiation in Water with Gas Bubbles: A Time Scale Approach

Nicholas L. Sponsel,[1] Sophia Gershman,[2] Maria J. Herrera Quesada,[1] Jacob T. Mast,[1] and Katharina Stapelmann[1, a)]

[1)] *Department of Nuclear Engineering, North Carolina State University, Raleigh, North Carolina 27695, USA*

[2)] *Princeton Plasma Physics Laboratory, Princeton, New Jersey 08536, USA*

(Dated: 21 August 2022)

High voltage nanosecond pulse driven electric discharges in deionized water with an argon bubble suspended between two electrodes were experimentally investigated. Two electrode configurations were used to temporally resolve the timescales of the discharge from the applied voltage rise-time (7 ns), through the end of the first pulse ($\sim$30 ns), and longer ($>$50 ns). We found that in positive and negative applied voltage polarities, discharge initiates in the water at the tip of the anode. The discharge in the water rapidly extends ($\sim 10^4$ m/s) to the apex of the bubble and light emitted from inside the bubble begins to form. The steep rate of rise of the applied voltage ($\mathrm{d}V/\mathrm{d}t < 4$ kV/ns) and the short time for the development of discharge in the water suggest that cavitation is a likely mechanism for discharge initiation and propagation in water. In addition, the short duration of the applied voltage pulse results in only a partial Townsend discharge inside the bubble.

[a)]kstapel@ncsu.edu

I. INTRODUCTION

Gas bubbles in water and other liquid dielectrics have been the topic of extensive theoretical and experimental research due to their ubiquitous presence in water disinfection[1,2], plasma machining[3,4], failing dielectrics[5,6], testing of composition of liquids[7,8] or the presence of impurities[9–11]. Gas bubbles may include intentionally injected gas used for water treatment, microbubbles that coalesce, and bubbles that expand thermally under long voltage pulses. The discharge in these complex systems can initiate at the electrodes, in bubbles attached to the electrodes, or bubbles floating in the liquid depending on the rate of rise and duration of the applied voltage.[12] Comparing the timescales of the plasma formation with the timescales bound by the applied voltage provides insight into the initiation and time sequence of the electric discharge processes. The discussion of discharge mechanisms below is presented according to a decreasing timescale from milliseconds, microseconds, hundreds of nanoseconds, down to nanoseconds.

Discharges in bubbles submerged in water are generally discharges at atmospheric pressure in the supplied gas (e.g., argon) with saturated water vapor. In a standard Townsend mechanism, electron avalanches form if a seed electron can gain enough energy in the electric field inside a bubble to result in an ionization event. The time for these processes is comprised of the delay time for the appearance of the seed electron and the formation of the initial and secondary avalanches. The initial delay time could range from microseconds to milliseconds depending on the mechanism producing the seed electron. The avalanche formation time is on the order of 10 ns, but the process can continue only if the formation of positive ions are not screened by the negative ions, and hence, the time is limited by the speed of ion drift in the applied electric field. If 1) the field (and thus the first ionization coefficient α) is high enough and 2) the bubble is large enough (typically, macrobubbles with diameters of $d \sim$mm) such that $\alpha d \sim 20$ (Meek criterion), then the discharge undergoes an avalanche to streamer transition. The streamer formation is limited by the negative ion drift velocity, v_i, and hence requires a time, $\tau = d/v_i$, of $\sim$100 ns. The total time of a partial breakdown in mm-sized bubbles is generally on microsecond timescales but may extend into the millisecond range due to the delay in obtaining a seed electron and in cases where the field is not strong enough for the avalanche-to-streamer-transition. These principles have been supported by extensive experimental work and modeling, as described below.

Many of the studies of electrical discharges in artificially introduced mm-sized bubbles have involved bubbles attached to an electrode or spanning the gap between the electrodes.[13–15] For example, 1 µs long voltage pulses with >100 ns rise-times, applied to mm and sub-mm size bubbles attached to electrodes, with imaging on ns to hundreds of µs timescales, have revealed discharges propagating along the surface of the bubbles; and on long timescales they observed resulting ripple surface oscillations and breathing volume oscillations of the bubbles.[13,16,17]

Kinetic modeling and experiments have shown that it depends on the ratio of the dielectric constants of the gas and liquid whether the streamer propagates along the gas-liquid interface or directly through the bubble.[18,19] For gas bubbles in deionized water, the high dielectric constant ratio of ∼80 corresponds to discharge propagation along the surface of the bubble due to a high tangential component of the electric field along the bubble interface boundary.[18]

Observations by Sommers and Foster of mm-sized bubbles trapped in an acoustic standing-wave, not in contact with powered electrodes and subjected to applied voltage pulses with a rise-time ∼100 ns, have demonstrated streamer development in water from a positive sharp electrode to the bubble, then followed by multiple streamers inside the bubble.[20] The subsequent deformation and physical breakup of the bubbles was followed through on a 10 µs timescale. Separately, Wang et al. investigated discharges in mm-sized bubbles under a maximum applied voltage pulses of $V(t) = 40\,\mathrm{kV}$ and a rate of rise of $\mathrm{d}V/\mathrm{d}t \approx 20$ kV/ms, as well as a maximum of $V(t) = 20\,\mathrm{kV}$ and a rate of rise of $\mathrm{d}V/\mathrm{d}t \approx 1$ kV/ns. The applied voltage pulses and bubble size are similar to our present experiment; however, the images presented by Wang et al. have exposure times of tens of microseconds, hence, the images integrate the entire history of the discharge and a time sequence is difficult to determine.[21]

In addition to the intentional introduction of macrobubbles, microbubbles on the scale of tens of µm can be observed. Microbubbles can be both intentionally introduced or naturally present in liquids. Naturally present microbubbles occur in liquids that have not been thoroughly degassed or after previous discharge cycles. Microbubbles have been observed to form throughout the liquid but are more likely to be found on the electrodes, especially on surface irregularities. The mechanism and the corresponding time delays for the discharge in water aided by microbubbles were first introduced by Korobeynikov.[22]

Microbubbles are filled with gas at atmospheric pressure; the discharge follows a similar

mechanism as that for macroscopic bubbles, except for the important effect of the size of the bubble on achieving the breakdown difference in potential between the ends of the bubble. Due to the small size of microbubbles, this is only achievable in the vicinity of the electrodes. Hence, the discharge is usually observed only in bubbles directly attached to the electrodes. Elongation of the bubbles, resulting in additional field enhancement, occurs prior to the initiation of the discharge. The timescale for the development of a discharge in microbubbles is on the order of 10^2–10^3 ns, a time comprised of the production of a seed electron, bubble elongation, and streamer development in the bubble. It should be noted that the production of a seed electron may take longer than the timescale mentioned above depending on the mechanism of origin, which remains the topic of continued investigations.

Microbubbles have been implicated in promoting electric discharge in liquid[22–27] by reducing the required breakdown field for discharges in liquids. In particular, they promote the initiation of the breakdown at the electrodes for discharges with applied pulse durations in the microsecond to sub-microsecond ranges. Bubbles with a radius of between 20–30 μm in fields up to 30 MV/m have shown primary streamers on a timescale of ∼100 ns, accompanied by deformation within ∼100–500 ns. Streamers entering water have been observed to develop in ∼1000 ns.[23] Introduction of <100 μm bubbles was found to reduce the minimum breakdown voltage between two electrodes submerged in water for ∼5 μs applied voltage pulses[26], similar to the earlier experiments and calculations by Korobeinikov[23] and Panov[25]. Few works have investigated the source of seed electrons needed for streamer development in bubbles. Babaeva et al.[27] have shown that streamers will not form in bubbles that are too small unless there is sufficient initial electron density, e.g. through preexisting charges if the observed discharges are not independent. Furthermore, it had been found that discharges in microbubbles can propagate through a stream of bubbles.

At nanosecond applied pulses, the processes mentioned above do not have enough time to develop. A faster mechanism has been proposed by Shneider and Pekker for discharge initiation on short timescales in strong and strongly inhomogeneous electric fields. This mechanism is based on the formation of reduced pressure regions in a liquid, a phenomenon called cavitation. Due to pressure fluctuations, nanometer-size voids (nanovoids) appear and collapse in a liquid, but a steep voltage rate of rise in an strong and inhomogeneous electric field can produce a net negative electrostrictive pressure. This negative pressure allows cavities to grow so that electrons can gain enough energy to produce ionization events.[28,29]

These works have shown that for an applied voltage rate of rise of several kV/ns, electrode radii of ∼25 μm, and electric fields of ∼200 MV/m, negative pressure of >30 MPa leads to the growth of nanovoids. Randomly appearing nanovoids grow to a size large enough to accelerate electrons to ionization energies in tenths of nanoseconds. This produces regions of enhanced electric field at the tip of the nanovoids. Electrons accelerate to ionization potential in the nanovoids and produce ionizations and excitations at the water boundary. The cavity can be filled with ionized and excited water molecules and fragments. The void, in turn, can serve as a sharp electrode to grow a new void. The total time to develop glowing regions starting with nanovoids can take ∼1 ns. Hence, in ∼10 ns, propagation of the discharge in water may be recorded.[12] This mechanism has been supported by the experimental evidence for ns pulsed discharges in degassed water with electrode radii <50 μm and a voltage rate of rise of ∼5 kV/ns.[30]

Recent experimental work by Šimek et al. has confirmed the previously reported results and shows that non-luminous structures develop 2–3 ns after the onset of the applied voltage pulse (50–150 kV, duration of ∼7 ns FWHM), followed almost instantaneously (∼100 ps) by luminous discharge events.[31] Computational investigation of electron multiplication and avalanching in nanovoids has shown that electron avalanches may be created by the emission of secondary electrons caused by a bouncing-like motion of electrons along the cavity.[32] In this case, the electron multiplication timescale was determined to be on the order of 1 ps or shorter, leading to a propagation velocity of the electron avalanche of about 2.8×10^6 m/s. Tereshonok et al. present a theoretical and experimental investigation of cavitation and bubble discharge mechanisms. The theoretical description demonstrates the applicability of the cavitation model to the description of discharge initiation at sharp electrodes and steep voltage rate of rise. In addition, they have emphasized that the dependence of dielectric constant of the liquid on the applied electric fields is as important as the voltage rate of rise and water conductivity.[33] The change in the dielectric constant with electric field increases the probability of cavitation development of the discharge. Most of the experimental investigations of the cavitation mechanism are concerned with prebreakdown processes in liquids, especially deionized water, subject to ns pulsed applied voltage.[34]

Discharges in ∼1 mm size argon, methane, carbon dioxide and propane bubbles in distilled water in a pin-to-pin geometry under an applied voltage of 15 kV — with an initial pulse 20 ns long and followed by damped oscillations up to 1 μs — were investigated by Hamdan

et al.[35] The experimental conditions of the above works are similar to those presented in this manuscript, but the time-integrated imaging of μs gate-widths does not reveal the details of the processes happening at the initiation and development of the discharge. In our investigation, the applied voltage pulse and the time resolution of the imaging make it possible to combine ∼5–500 ns timescales.

This manuscript presents an experimental study that addresses discharge initiation and propagation in water with Ar macrobubbles subject to pulsed non-uniform electric fields. The combination of a maximum applied voltage rate of rise of ∼4 kV/ns and subsequent voltage oscillations, sharp electrodes, and a macrobubble positioned accurately between the electrodes during the discharge produces a situation where processes that occur on different time scales become tractable. Therefore, we present a phenomenological picture of each process: from the initiation of the discharge, through its propagation from the positive electrode to the bubble, through emission in the bubble, and effects of the electrode polarity. Our imaging and electrical data demonstrate the complex processes that occur during discharges in this multiphase medium at nanosecond to several hundred nanosecond timescales.

The order of the paper is as follows. We start by describing our experimental methodology addressing bubble geometry and timing methods. For the first time, we present an original method of bubble positioning with control of statistical information of the bubble shape, size, and position between the electrodes. A unique timing scheme is introduced that allows the application of the voltage pulses when a bubble is in the desired position between the electrodes. Finally, the experimental results and discussion section present our evidence for the discharge initiation for two electrode configurations by order of timescale.

II. EXPERIMENTAL METHOD

A. Experimental Setup

The experimental setup was designed to reliably capture free-flowing bubbles between electrodes synchronously with an applied high-voltage (HV) ns-pulse. It consists of a rectangular quartz vessel filled with deionized water and two tungsten/copper alloy electrodes positioned horizontally. Argon gas passes through a horizontal capillary running along the

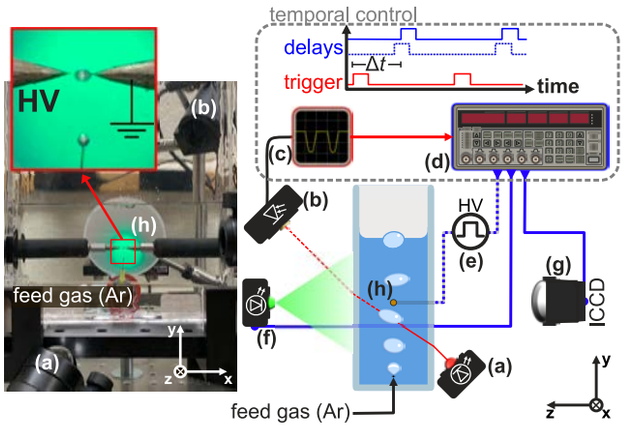

FIG. 1. Front image and cross-sectional illustration of the experimental setup and triggering system comprised of: (a) collimated 740 nm LED, (b) Si photodetector, (c) oscilloscope, (d) delay generator, (e) HV ns-pulse generator, (f) 530 nm LED backlight, (g) ICCD, and (h) tungsten/copper electrodes. The delay generator (d) controls the vertical position of the bubble between the electrodes (h). Backlit "stationary" bubbles discernible with human eye or consumer-grade camera.

bottom of the vessel parallel to the electrodes as shown in the image and illustration of Figure 1. Two different electrode geometries are used for the experiments: 1) a sharp-to-sharp and 2) a sharp-to-flat configuration. Gas bubbles exit a vertical hollow needle affixed to the capillary resulting in bubbles with a diameter of 1.7 ± 0.1 mm (Figure 2). The hollow needle is aligned so that the bubbles pass between the electrodes. The depth of the water and the gas flow are adjusted to achieve a desired speed and frequency of bubbles as they rise. The argon flow rate of 1 mL/min results in a bubble-detachment frequency of $5.60 \pm 0.03\,\mathrm{s}^{-1}$ under our conditions. The direction of the bubble flow-path depends on bulk gas velocities in the bubble as addressed in detail in our previous work.[36] The triggering system can operate at the bubble-detachment frequency (see Section II B below); however, every HV pulse and image in this experiment is performed using manual single-shot triggering executed off of the subsequent bubble. Single shot triggering ensures that each discharge is an independent event that occurs under the same initial conditions.

Different regimes of bubble deformation are catalogued along the bubble's travel-path after bubble detachment from the hollow needle. A region of stability immediately after the bubble detachment is utilized to achieve highly elliptical bubbles and to control bubble eccentricity, $e = (1 - b^2/a^2)^{1/2}$, where a is the bubble major radius and b is the bubble

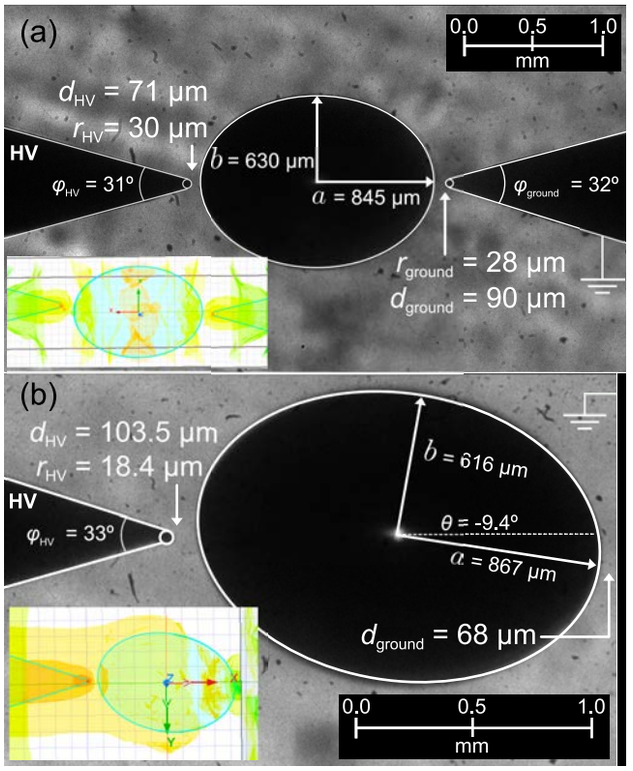

FIG. 2. Geometry and dimensions of sharp-to-sharp and sharp-to-flat tungsten/copper electrode configurations including electrode cone angle (φ_{el}), distance from electrode to bubble apex (d_{el}), radius of electrode tip (r_{el}), and bubble major (a) & minor (b) radii. Electrode subscript specifies which electrode is in reference (el → HV/ground). Sharp electrodes have an average tip radius of $28 \pm 7\,\mu$m. Distance between the electrodes and the bubble's apex is on average $89 \pm 62\,\mu$m. Dimensions of images (a) and (b) used for ANSYS Maxwell models to investigate field properties, depicted on the inserts.

minor radius (Figure 2). Moving the opening of the needle closer to the electrode gap, such that bubble travel distance decreases, results in decreasing bubble eccentricities. To measure bubble parameters a MATLAB script was written to fit each bubble to an ellipse and quantify its position, major & minor diameters, areas (pixel-counted and fitted), eccentricity, and angle with respect to the horizontal pixel arrays.[36] The results of this analysis for several images are included in Table I. See supplementary material at [URL will be inserted by AIP Publishing] for images and values of the bubble statistic results in Supplementary Section A.

Source	Uncertainty
Optical Measurements	*(Spatial Resolution)*
Caliper Precision	10 μm
Imaged Pixel Width	4.4 μm (sharp-sharp) 2.5 μm (sharp-flat)
Imaged Bubbles Statistical: N=50	position $\sigma_x = 10$ μm $\sigma_y = 3$ μm diameter $\sigma_a = 3$ μm $\sigma_b = 3$ μm
Electrical Measurements	*(Temporal Resolution)*
SRS DG645 Rubidium timebase	1 ns
Pearson Current Probe	5 ns
Textronix HV Probe	4.67 ns
Andor iStar ICCD	0.035 ns (jitter)
Gate Signal	2.7 ns (statistical)
MegaImpulse Pulser	1 ns

TABLE I. Uncertainties propagated across experimental conditions including statistical analysis, manufacturer's specifications, and tool precision. Spatial uncertainty is associated with imaging measurements and temporal uncertainty is associated with electric measurements.

B. Optical Triggering

A significant difficulty in ns discharge experiments, with detached gas bubbles in a liquid, is triggering the applied voltage pulse at a specific bubble position and triggering the diagnostics at the desired time during the discharge. We overcome this difficulty by an original optical triggering system based on the free-flowing vertical motion of a stream of bubbles. Our triggering system aligns the electrical and optical parts of the experiment temporally and spatially. Figure 1 shows a photo of the system from the perspective of the ICCD and a cross-sectional diagram of the triggering system. A collimated LED ((a) Thorlabs M740F2 740 nm) is aligned such that its beam passes below the electrode gap and terminates at a

photodetector ((b) Thorlabs DET36A2 Si Detector) on the other side of the quartz water vessel. The attenuated signal produced by a bubble obfuscating the path of light is transmitted to an oscilloscope ((c) Tektronix MDO3104) which is set to trigger at the falling edge of the incoming signal. The oscilloscope monitors both the bubble frequency and stability. It is then used as the external trigger for a delay generator ((d) SRS DG645: Rubidium timebase) that calibrates timing for the remaining elements.

The vertical ($y-$axis) bubble position between the electrodes is controlled by delaying the outgoing signal from the delay generator. Three separate delays are routed to a HV nanosecond pulse generator ((e) Megaimpulse NPG-18/100k), LED backlight ((f) Thorlabs M530F2 530 nm), and ICCD ((g) Andor iStar 734). Pixel-to-μm conversions were calibrated by imaging a thin wire with a diameter of 450 μm (Table I) between the tips of the electrodes.

C. Electrical Measurements

A HV generator (pulser) with external triggering capabilities applies a ns voltage pulse to a submerged sharp electrode while the other electrode (sharp or flat) is grounded. An equivalent circuit of the power source, the bubble/electrode gap, and measurement devices is shown in Figure 3. The electrical characteristics of the experiment were measured with a HV probe (Tektronix P6015A (75 MHz)) and inductive current monitor (Pearson Model 6600) measured with a 5 GS/s Oscilloscope (Rigol DS6104, 1 GHz, 5 GS/s).

Further time calibration between the HV probe and current monitored due to circuit phase delays are carried out by simulating the equivalent circuit for all experiment components (Figure 3). The large distance (~ 2 mm) and small area ($\sim 56\,\mu\text{m}^2$) of the electrode gap leads to the concern that reactive elements of the measuring devices in the circuit may have a significant effect on the electric measurements of the system. In particular, if the reactance of the current monitor, $X_{\text{current}} = \omega L_{\text{current}}$, is similar to or larger than the magnitude of the electrode reactance, $X_{\text{el}} = -(\omega C_{\text{el}})^{-1}$, the current recorded from the monitor could be delayed on the ns timescale. An equivalent circuit model is simulated in LTspice to determine temporal delay introduced by measuring devices acting as part of the total circuit. To accurately determine the capacitance of the bubble/electrode circuit element, a 3D model of each geometry in Figure 2 was modeled in ANSYS Maxwell field solver. An overall additional delay of 1.5 ns is added to the cable delay based on the results of the

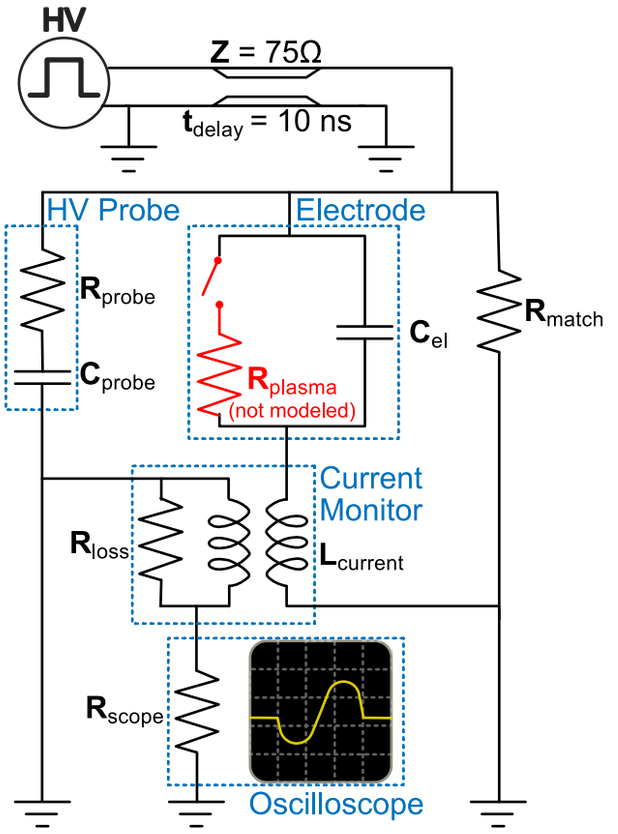

FIG. 3. Equivalent circuit model of the experiment simulated with LTspice. The pulse generator and transmission line (cable) have an impedance of 75 Ω. The HV probe is modeled as an RC element ($R_{\text{probe}} = 100\,\text{M}\Omega$, $C_{\text{probe}} = 3\,\text{pF}$). The electrode gap is modeled as a capacitor ($C_{\text{el}} = 3\,\text{pF}$), while plasma resistance is not included in the model. Matching power resistor placed in parallel to electrode ($R_{\text{match}} = 74\,\Omega$). The current monitor is modeled as a pair of coupled inductors with a core-loss resistance ($L_{\text{current},1} = L_{\text{current},2} = 10\,\mu\text{H}$, $R_{\text{loss}} = 200\,\mu\Omega$) terminated to a 1 MΩ oscilloscope.

LTspice circuit model with the measurement devices included in the equivalent circuit and the electrode/bubble gap capacitance determined from the ANSYS model (2.0 pF for the sharp-to-sharp configuration and 3.1 pF for the sharp-to-flat configuration). The HV probe parameters, $R_{\text{probe}} = 100\,\text{M}\Omega$, $C_{\text{probe}} = 3\,\text{pF}$, are from the manufacture's description. See supplementary material at [URL will be inserted by AIP Publishing] for electric field models for electrode configurations. Current monitor inductance, $L_{\text{current}} \approx 10\,\mu\text{H}$, is determined by sweeping through inductance values ($10\,\text{nH} < L_{\text{current}} < 50\,\mu\text{H}$) in the LTspice model

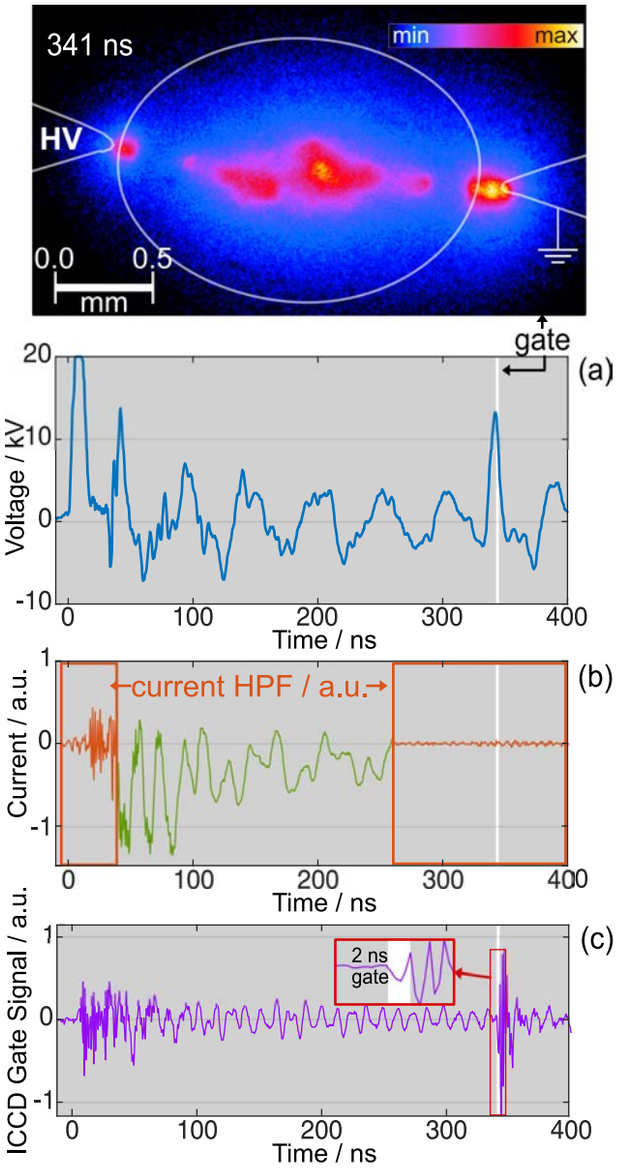

FIG. 4. Oscilloscope traces for HV ns-pulse applied to free-flowing bubbles. (a) Applied voltage trace, (b) current (green) overlaid with a 100 MHz high-pass filter (HPF), and (c) ICCD gate signal are overlaid with the image gate associated with the bubble image (not shaded). Uncertainty for gate timing $\sigma_{\text{gate}} = 2\,\text{ns}$.

and fitting simulated current to measured current. The core-loss resistance of the current monitor, $R_{\text{loss}} = 200\,\mu\Omega$, is modeled in parallel with the coupled inductor in the circuit.[37] Power spectrum analysis of the measured pulser applied voltage and reflections result in a dominant reflection frequency of $f_{\text{pulse}} = 14\,\text{MHz}$. Under this condition the circuit remains

significantly capacitive ($X_{\mathrm{el}} = -4.5 \pm 0.9\,\mathrm{k\Omega}$; $X_{\mathrm{current}} = 0.8\,\mathrm{k\Omega}$). See supplementary material at [URL will be inserted by AIP Publishing] for simulated currents of varying inductances in Figure S7.

The time-corrected oscilloscope traces used for aligning optical results to electrical results is exemplified by Figure 4. The applied voltage (Figure 4(a)) sharply rises to $20 \pm 1\,\mathrm{kV}$ from 5%–95% peak value over $7.0 \pm 0.5\,\mathrm{ns}$ ($\mathrm{d}V/\mathrm{d}t = 2.6 \pm 0.3\,\mathrm{kV/ns}$). The characteristic shape of the HV pulse consists of two rise-time sections separated by a 1 ns plateau at 11 kV. The voltage rate of rise for each steep rise is $3.7 \pm 0.8\,\mathrm{kV/ns}$. The peak is followed by a slower fall of $18.5 \pm 1.5\,\mathrm{ns}$ from 95%–5% peak value. The width of the pulse is measured at full-width-half-max and is averaged to be $16.1 \pm 4.9\,\mathrm{ns}$. The first maximum occurs $\sim 9.0 \pm 0.5\,\mathrm{ns}$ after the initial steep voltage rise-time, which is measured to begin at $\sim 5\%$ peak voltage. The beginning of this voltage rise-time is defined as the temporal origin for all ICCD gate references hereafter. The bubble position and size change the reactance of the system and can influence the reflections of the pulse. See supplementary material at [URL will be inserted by AIP Publishing] for impedance estimations and power spectrum of the voltage waveforms in Supplementary Section B.

The reflected oscillations decay with a characteristic decay time of $\tau_{\mathrm{pulse}} = 300 \pm 80\,\mathrm{ns}$. The raw current traces (outlined in green, Figure 4(b)) are processed with a high-pass filter (HPF) attenuating frequencies below 100 MHz (orange box). This is done to clearly distinguish the high-frequency current oscillations associated with the electromagnetic interference accompanying large discharges.[38] The HPF box is placed at the beginning and end of the current trace in Figure 4 to demonstrate the difference between these current traces. In this manuscript the current trace is used for timing purposes and will only be presented with the applied HPF with arbitrary units. Figure 4(c) shows the ICCD gate signal output in relation to the voltage and current peaks, and both the gate delay and gate-width values are indicated on each image. In this manuscript, the gate-width is presented as the unshaded section of the oscilloscope trace.

The electrode gap is set up by aligning tips as close to the bubble apex as possible, given that the bubble travel-path is established first. After ~ 30 discharge events, degradation in the electrode is detected by persistent discharge attenuations. To investigate the influence of small variations in the distance between the electrode and gas bubble, d_{el}, the E-field simulations modeled in ANSYS Maxwell are used. For the average bubble positioned be-

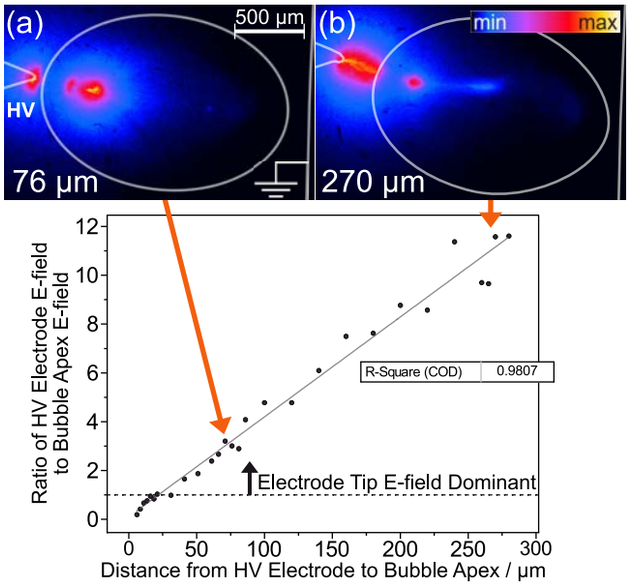

FIG. 5. Ratio of the E-field at the HV electrode tip to the E-field of the gas/liquid bubble apex boundary simulated via ANSYS for varying bubble distances, d_{el}. A minimum distance of $24 \pm 8\,\mu\mathrm{m}$ corresponds to a reversal of dominant field strength from bubble apex to electrode tip E-fields. For the corresponding images, the camera gate is opened prior to the HV pulse and closed at (a) 15 ns and (b) 17 ns after the initial applied voltage rise-time. Uncertainty for gate timing is $\sigma_{\mathrm{gate}} = 2\,\mathrm{ns}$.

tween two sharp electrodes, small variations in horizontal displacement do little to alter the magnitude of the E-field directly at the electrode tips. However, when a bubble drifts too close to the sharp electrode tip, or when d_{el} grows too large, the difference between the E-fields at the boundary interfaces have a noticeable effect on the emission behavior. The ratio between the E-fields at the HV electrode tip and the left bubble apex is plotted in Figure 5 for the sharp-to-flat configuration.

The simulation shows a critical distance from the electrode at which the magnitude of the E-field is larger inside the bubble apex boundary than at the electrode tip ($d_{\mathrm{crit}} = 24 \pm 8\,\mu\mathrm{m}$). After this distance, the ratio between the E-fields increases linearly up to the point of contacting the flat grounded electrode. Images from this electrode configuration observed around the similar time frames show evidence of this distinction. Figure 5(b) is chosen from an image gated 2 ns after Figure 5(a) to account for the time taken to propagate a longer distance through water. Figure 5(a) is positioned such that the bubble apex is 76 µm from

the HV electrode tip and shows similar magnitudes of electrode tip emission and emission observed within the gas region of the bubble. By contrast, Figure 5(b) measures a bubble apex distance 270 μm away from the electrode tip, and tip emission is significantly greater than that in the bubble region emission. As shown by the simulation, at this distance the electrode tip field is over an order of magnitude greater than that at the bubble apex. Bubbles chosen for temporal-resolution results fall within a stable region in which electrode tip E-fields remain within an order of magnitude. See supplementary material at [URL will be inserted by AIP Publishing] for details of the electrostatic simulations and analysis for our electrodes.

III. RESULTS AND DISCUSSION

In this work, we examine the initiation of a discharge in deionized water with and without an Ar bubble between the two electrodes on time scales from nanoseconds to several hundred nanoseconds. We demonstrate that for two electrode configurations — sharp-to-sharp and sharp-to-flat electrodes — and for both applied voltage pulse polarities, the discharge originates at the tip of a sharp positive electrode. A glow at the tips is a persistent feature of our observations. A partial discharge was also observed in the Ar bubbles at certain times of the pulse. Finally, images taken ∼100 ns later in the discharge present the appearance of the discharge bridging the gap between the electrodes within the argon bubble. We show below that this appearance does not mean that the discharge propagates from one electrode to another, but rather that it originates at different times at each sharp electrode. A timescale approach is utilized in presenting the following results: first, we present and discuss images taken during the voltage rise prior to it reaching its maximum value; then we present the images corresponding to the time when the first pulse is falling; and finally we discuss emissions detected in regions of oscillating pulse decay on longer timescales.

A. Nanosecond Pulse Timescale: The Rise

The earliest images taken within the first nanoseconds of the start of the applied voltage pulse show light emission at the tip of the anode. Figure 6 shows examples of repeated images of the tips of the sharp-to-sharp electrode configuration. To detect the earliest light,

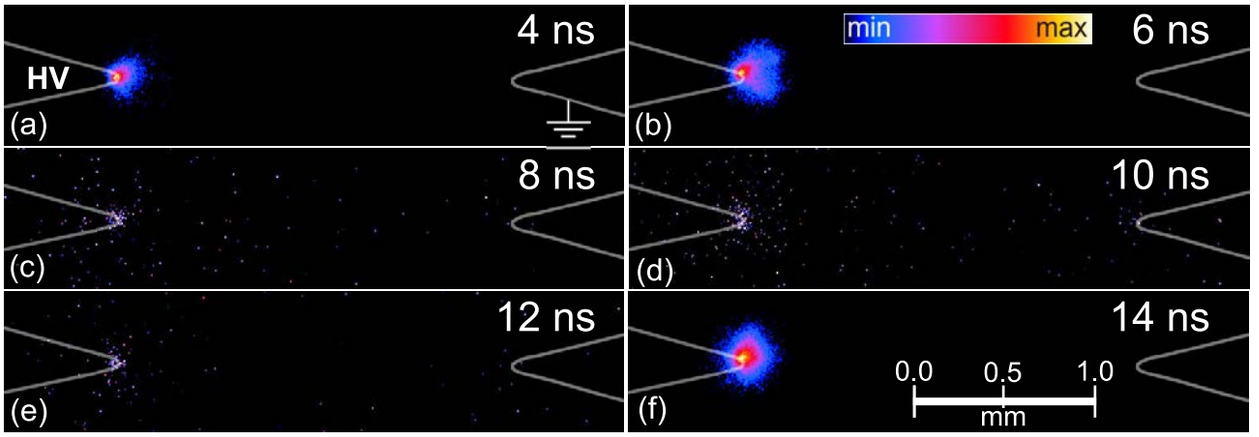

FIG. 6. Two sharp electrodes without gas bubbling through the water. The glowing region is visible at the tip of the HV electrode. The camera's gate width is for 2 ns and stepped in 2 ns intervals. The time: (a) 4 ns , (b) 6 ns, (c) 8 ns, (d) 10 ns, (e) 12 ns, (f) 14 ns, is estimated from the start of the voltage pulse shown in Figure 4. Uncertainty for gate timing is $\sigma_{\text{no gate}} = 4$ ns.

the ICCD gate (width of 2 ns) was backed up to the time prior to the start of the applied voltage pulse and then advanced in 2 ns time steps until a glow was observed. Repeated images were captured under the same conditions without changing any of the camera or pulser settings. The images show a glowing discharge region that appears to develop at the tip of the HV electrode, then extinguishing and possibly reappearing again. There are no collection of oscilloscope measurements corresponding to each individual image; instead the timing is calculated between the ICCD activation signal and the HV pulse from the initial measurement of this data set, resulting in a larger temporal uncertainty than images presented with argon bubbles. See supplementary material at [URL will be inserted by AIP Publishing] for traces of the activation signal (Figure S6). Considering the experimental uncertainties, these observations demonstrate the appearance of a glow at the tip of the positive HV electrode in the absence of injected gas. For all the gate delays shown in Figure 6, the glow is observed within the time of the first voltage pulse and appears to originate within ± 5 ns of the peak voltage.

In addition, the glow at the tip of the electrode is also observed when Ar gas is bubbled through the water. As described in Section II, the applied voltage pulse is timed so that a bubble is positioned between the electrodes. It remains practically stationary during the $\sim$500 ns of the first voltage pulse and subsequent decaying oscillations. The uncertainty in

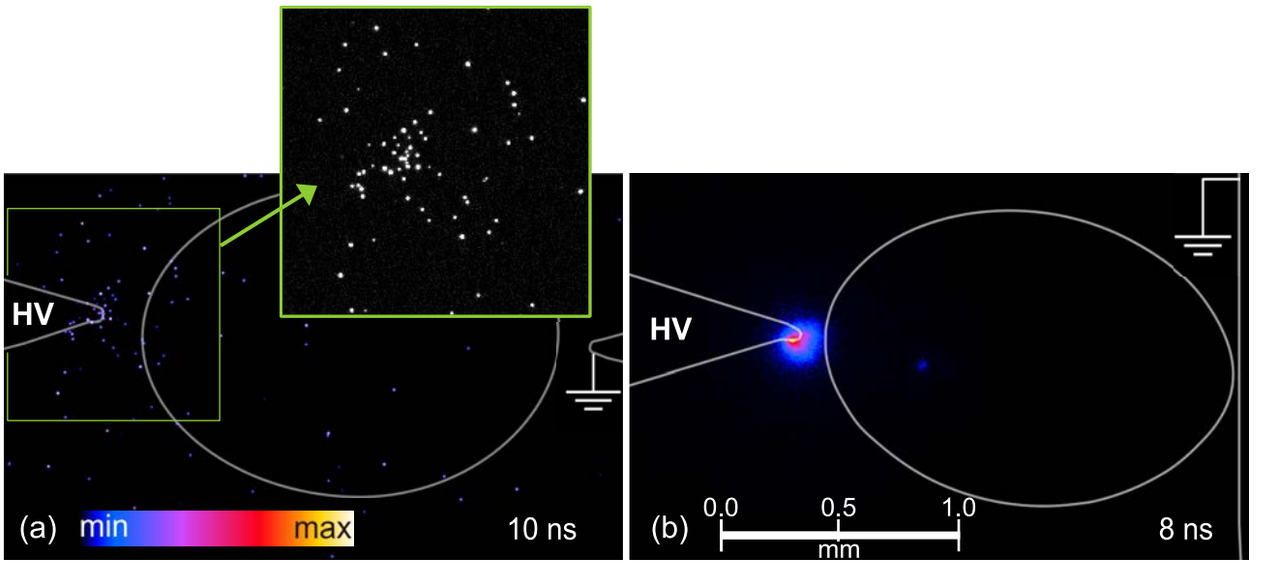

FIG. 7. Images taken immediately after the voltage reaches its maximum value show faint glow at the tip of the HV electrode. Emission detected with a 5 ns gate-width for (a) sharp-to-sharp configuration at 10 ns, and (b) sharp-to-flat configuration at 8 ns after pulse rise. Uncertainty for gate timing $\sigma_{\text{gate}} = 2$ ns.

bubble position is 10 μm (Table I). Figure 7 shows that a faint glow at the tip occurs at the positive HV electrode and is captured before the bubble itself begins to glow. The glow at the tip of the sharp electrode occurs independent of the electrode configuration and has also been observed in the sharp-to-flat electrode configuration as well (Figure 7(b)).

All the observations discussed so far present images taken within several nanoseconds of the applied voltage pulse reaching the first maximum. The most prominent feature of the images taken on various time scales in our experiments is the glow observed at the tip of the electrodes. This glow is observed with and without the involvement of a macrobubble. However, it should be considered that the water is not degassed and could contain microbubbles due to the dissolved air in a container open to the atmosphere. Small irregularities in the electrode could contain pockets of gas (likely a mixture of air, argon, and water vapor) and form microbubbles with a size of ∼1 μm. Smaller bubbles cannot be sustained in water at atmospheric pressure (Shneider and Pekker, p.57)[12] and larger bubbles would be detected in the backlit images. Therefore, we will begin the discussion of the rationale for the glow initiating at the tip of the electrode submerged in water with the possibility of the discharge

initiating in a microbubble.

Gas discharges occur if the field exceeds the minimum required by the value of pd, a product of the gas pressure, p, and the size of the gas gap, d, which in this case is the size of the bubble. The small size of the bubble is responsible for a very small pd value of $\sim$0.1 Torr cm; this is lower than the pd minimum for the gasses in our system. Hence, this breakdown would require a potential difference, ΔV, of $\sim$1 kV across the bubble. The electric field immediately next to the electrode is:

$$E(r,t) = \frac{V_{\max} r_{\mathrm{el}}}{r^2} \frac{t}{t_{\mathrm{o}}}, \tag{1}$$

where $V_{\max}$ is the maximum applied voltage, t is the time from the start of the voltage pulse, t_{o} is the voltage rise-time, r is the distance from the electrode tip, and r_{el} is the radius of the electrode tip. For $V = 20$ kV, $r_{\mathrm{el}} \approx 26\,\mu$m, $t_{\mathrm{o}} \approx 6$ ns, $t = t_{\mathrm{o}}$, and $r = r_{\mathrm{el}}$, $E \approx 8$ MV/cm. This is an estimate of the maximum value of the field immediately next to the electrode at its tip and it agrees within an order of magnitude with the ANSYS simulation of $E \approx 3$ MV/cm. Both values fall short of providing the required kVs across a microbubble. This means that even if an electron accelerated in the applied field, with a mean free path at atmospheric pressure of $\sim$0.1 μm, the microbubbles are too small to develop well-formed electron avalanches. In addition, to grow a microbubble would involve thermal processes that take microseconds, not nanoseconds, to develop (Shneider and Pekker, Chp.9).[12] Hence, we conclude that the observed discharge must initiate and develop by a different, faster, mechanism that also allows for a possible quick expansion of the glowing region. As shown in Figures 6 & 7, the light from the region next to the electrode tips is recorded at or before the voltage reaches its maximum value of $t = 9$ ns.

Discharge initiation by cavitation requires a pulsed nonuniform electric field and depends strongly on the electrode tip radius of the electrode and the applied voltage rise-time. Experimental[30] and theoretical[6,28,29] work have shown that cavities can develop and grow when the electrode tip radius is $\sim$30 μm and the voltage rise-time is <10 ns. In this work the electrode tips have radii of $28 \pm 7\,\mu$m, an average voltage rate of rise is 2.6 ± 0.3 kV/ns, and the total time to reach peak voltage of about 9 ± 1 ns. Under these conditions, electrostrictive cavitation is feasible, and spontaneously formed nanocavities can grow to enable ionization and discharge initiation.[12] Experimentally, cavitation was reported by Dobrynin et al.[30] for negative electrostrictive pressure of $\sim$30 MPa. If we use the electric field near

the electrode estimated above, the negative electrostrictive pressure produced close to the electrode is

$$|P_{-}| = \frac{1}{2}\alpha\varepsilon_{\rm o}\varepsilon E^2 > 30 \text{ MPa}\,, \tag{2}$$

for $3 < t < 7$ ns for all experimentally measured radii of sharp electrodes. In equation (2) α is an empirical factor for a dielectric liquid, $\varepsilon_{\rm o}$ is permitivity of free space, and ε is the relative dielectric constant of the liquid. For water, $\alpha = 1.5$, $\varepsilon = 81$, and E is estimated from equation (1). As stated above, light from the electrode region is observed as early as 6–8 ns after the start of the voltage pulse. This time is insufficient for the bulk water to move in and compensate for the negative pressure in the void. Moving at a speed of several meters per second it requires hundreds of nanoseconds to move 1 μm — a much greater time than the observed glow at the electrode tips. On a ns timescale, the bulk water does not have time to respond and the cavity can continue to expand. Nano-scale cavities are naturally present in bulk water, but their expansion requires sufficient negative pressure. The expansion of a nanocavity is necessary because there needs to be sufficient distance for an electron to acquire enough energy to produce ionization. The minimum energy required is >12.6 eV, the ionization energy of water molecules. Assuming that the negative pressure in the cavity is sufficient to move the water, the speed of expansion can be estimated as

$$v_{\rm exp} \approx \sqrt{\frac{2|P_{-}|}{3\rho}}\,, \tag{3}$$

where P_{-} is the negative pressure from equation (2) and ρ is water density. For a seed electron accelerating in the E-field inside the cavity to gain 12.6 eV, the size of the cavity should be $R(t)$, such that

$$12.6 = e\Delta V = 2eER(t) \approx 2eE\sqrt{\frac{2|P_{-}|}{3\rho}}t_{\rm ion}\,, \tag{4}$$

where $t_{\rm ion}$ is the time needed for a cavity to expand sufficiently such that an electron can gain 12.6 eV. This expression results in an approximate time of, $t_{\rm ion} \approx 0.5$ ns. Hence, at our applied voltage rate of rise and amplitude, the voids expand and the electrons in the voids gain sufficient energy for ionizing water molecules on a timescale shorter than the voltage rise-time. After electrons sink into the anode, a virtual electrode is formed by the positive ions, and the cavitation process can continue. The basic criterion for the applicability of the cavitation approach is that the rise-time of the applied voltage must be shorter than the time

required for new water to fill in the region close to the electrode where voids can grow, as discussed. The size of the region depends on the applied voltage and following estimations in Shneider et al.[28], is approximately $R = 1.5\ r_{\mathrm{el}}$. For our electrodes, $R \approx 40\,\mu\mathrm{m}$, water moving at the speed of sound of 1500 m/s would take $\sim$25 ns to be displaced. Hence, the rise-time of the applied voltage pulse in this work is well within the required limits. The time scale estimates here show that the conditions needed for the cavitation model to hold are satisfied in our experiments.[12] The cavitation model was first proposed theoretically in Shneider et al.[28] and further developed in the author's monograph.[12] Observations by Pekker[39], and Dobrynin et al.[30] provide experimental evidence for this model and more recent detailed studies[40,41] further validate this it. Moreover, Grosse et al. applied a voltage pulse of very similar characteristics to the one presented here in our work to deionized water using a 50 µm radius tungsten wire electrode. Cavitation theory was used to simulate the cavity growth and the results were consistent with experimental observations using shadowgraphy and optical emission spectroscopy (OES).[40]

Our work contributes to the evidence in favor of the cavitation model but does not directly address the origins of the first electrons. The question on the first electron persists because the usual mechanisms such as cosmic radiation, for example, require a wait time that is too long for the ns pulsed discharges. Other sources have been proposed but are difficult to confirm through direct experimentation. Zhang and Shneider[42] show that electron detachment from the hydroxide ion at the surface of cavities may be the most probable source of the initial electrons and also propose a scheme for discharge propagation from one cavity formed by electrostriction to another. We will return to the propagation scheme for later timescales after reporting additional observations occuring within the first applied voltage pulse.

B. Nanosecond Pulse Timescale: The Fall

On this intermediate timescale during the decay of the first half-wave of 12–30 ns, we report two main observations: 1) a glow at the electrode tip that extends to the bubble, and 2) a light forming in the bubble. Images taken with 10 ns and 14 ns delay times with a 2 ns gate width (Figure 8) in sharp-to-sharp electrode configuration show the glow region extending from the electrode tip to the apex of the argon bubble. Similarly, images presented

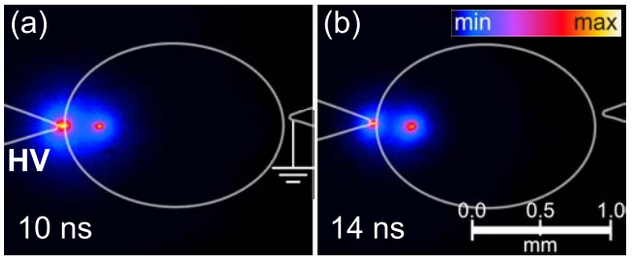

FIG. 8. Images of a discharge from the tip of the electrode reaching the apex of the bubble. These images also show a glowing region inside the bubble. The delay times are (a) 10 ns and (b) 14 ns and gated for 2 ns. Uncertainty for gate timing $\sigma_{\text{gate}} = 2\,\text{ns}$.

in Figure 5 show the glow region extending from the electrode tip to the bubble apex in the sharp-to-flat electrode configuration. In some images, as in Figure 10(a), the discharge appears to extend from the side of the electrode tip which may be a consequence of this being the closest distance and/or a local irregularity on the surface of the electrode. This underscores the 3-dimensional nature of the discharge path and the approximate nature of the velocity estimates. Although the error in the bubble position is only $\pm 10\,\mu\text{m}$, the three dimensional character of the bubble introduces additional uncertainty.

To estimate the velocity of the propagation, images that show the glow just appearing inside the bubble can be used for an approximation. From the images in Figure 8, the propagation time can be estimated as $\sim$10 ns. The distance between the electrode tip and the bubble apex were measured from the back lit images of the bubble-electrode arrangement and hence, from a flat projection of the bubble-electrode arrangement. With this limitation, the distance between the tip of the electrode and the apex of the bubble was estimated as $\sim 100\,\mu\text{m}$. The speed of propagation of the discharge from the tip to the bubble is thus $< 10^4\,\text{m/s}$, consistent with Figure 5 (b) which yields $< 2 \times 10^4\,\text{m/s}$ ($270\,\mu\text{m}$ distance, 17 ns). Considering the measured uncertainty of our estimations, this speed is in good agreement with the speed of propagation for ns pulsed breakdown in water reported previously by Grosse et al. ($4.6 \times 10^4\,\text{m/s}$)[41] and Ceccato et al. ($3 \times 10^4\,\text{m/s}$)[43].

Considering the time it takes for the discharge from the electrode tip to reach the apex of the bubble, a very fast mechanism is needed. As discussed, these fast mechanisms could be propagation by cavitation as proposed in Shneider and Pekker[12], and further developed in the recent works[42]; or by producing an E-field strong enough for the production of local

electrons inside the bubble to initiate the avalanche process. In the cavitation propagation mechanism, a nanovoid or cavity elongates to the size sufficient to accelerate the electrons to the energies sufficient for ionization, as described above. These energetic electrons ionize water molecules. Once the newly generated electrons reach and sink into the anode, the cavity acquires a positively charged head and becomes a new sharp anode that initiates a new cavitation process. Since electrons take ps to move through the cavities, the overall process across micrometer will take ns to complete.

The second observation for this timescale is the appearance of the glow in the Ar bubble injected between the electrodes. For a breakdown to occur in the bubble, the field must exceed the minimum breakdown field corresponding to the value of pd as usual in gas discharges. For a 1.7 mm bubble with Ar gas inside at atmospheric pressure, $pd \sim 100$, which is a large pd that requires a field on the order of >10 kV/cm. For both geometries in our experiment, $r_{\rm el} \ll d_{\rm el}$, and certainly much smaller than the distance between the electrodes. The electric field in the vicinity of the bubble for a 20 kV applied voltage and a 0.2 cm inter-electrode gap ($\sim 300\,$kV/cm) is roughly $\times 10$ the breakdown voltage. Hence, conditions are met for the discharge to start during $\sim 10-15\,$ns of the first applied pulse, or until the voltage falls below 1/10 of the max peak value. Under these conditions, $E/p \sim 400$ V/cm/Torr, and

$$\frac{\alpha}{p} = A \exp\left[-\frac{B}{E/p}\right], \tag{5}$$

where (for Ar), $A = 12$ (cm Torr)$^{-1}$, $B = 180$ cm Torr (Raizer, Russian edition, p. 150, table 5.1)[44] which gives $\alpha \approx 6000$ cm^{-1} and $\alpha d > 20$ for mm bubbles. This is a very large value of the first ionization coefficient meaning that the expression used for this estimation may not hold for large electric fields. For a mm size bubble, the condition of $\alpha d > 20$ would be satisfied for $\alpha \approx 200\,$cm^{-1}. This means that there is a likelihood of streamer discharge in an Ar bubble situated between the electrodes provided that there are seed electrons present and if there is enough time for the avalanche to streamer transition. This transition is determined by the negative ion drift velocity because removal of negative ions is required for field enhancement at the head of the streamer. Ion drift velocity is $\sim$1000 m/s and, therefore, the time needed is on the order of microseconds. Hence, the time of the applied voltage pulses of $\sim 30\,$ns is insufficient for streamer formation and the discharge remains in the Townsend mode. The sharp-to-flat electrode configuration gated to capture the entire first half-wave of the initial pulse exhibits a similar behavior with only a diffuse glow present

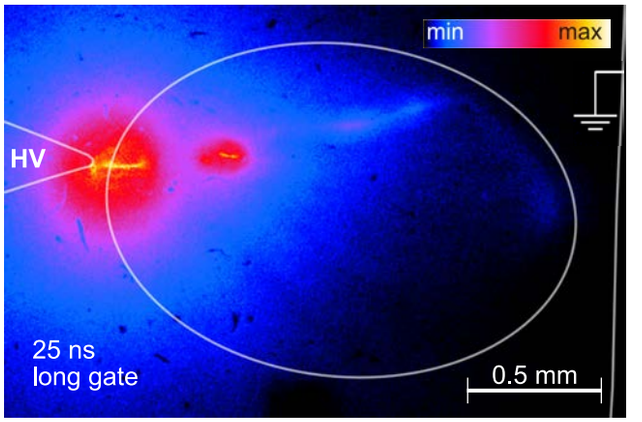

FIG. 9. Image of bubble between sharp-to-flat electrode configuration. Gate width opened from 175 ns before, to 25 ns after, the HV pulse rise-time. Emission detected display diffuse structure forming across bubble at this timescale, but occurs at the end of the initial applied voltage pulse. Uncertainty for gate timing $\sigma_{\text{gate}} = 2$ ns.

in the bubble. Figure 9 captures light emitted over the first 25 ns after the initial applied voltage pulse rise-time. The expansion in this mode can be estimated as the speed of the ionization front and is $\sim 10^4$ m/s, so the glow is expected to extend about 0.3 mm in 30 ns which falls short of the 1.7 mm across the bubble.

Estimations and ANSYS modeling also show that the electric field inside the bubble depends on the position of the bubble relative to the HV electrode. In cases when the bubble is closer, the discharge in the bubble may initiate sooner and is visible at earlier times together with the glow at the tip of a HV electrode. If the bubble is further away from the HV electrode, the glow may initiate at later times relative to the start of the applied voltage pulse. The fast streamer-like extension of the discharge region from the HV electrode may be acting as an extension of the anode and increasing the field inside the bubble. Therefore, the glow in the bubble may be delayed and seem to appear when the glow region from the electrode tip extends toward the bubble.

To summarize, in the intermediate time regime of 12–30 ns, when the images are taken during the decay of the first half-wave, the discharge in the water is observed to span the region between the tip of the anode and the apex of the bubble, eventually appearing in the bubble. The fast propagation toward the apex of the bubble requires a fast mechanism such as cavitation propagation. The discharge in the gas bubble does not have time to develop

into a streamer, although the electric field is strong enough, and remains in the Townsend mode which accounts for the diffuse character of the observed glow inside the bubble.

C. Evidence of Anode-initiated Breakdown

Experiments were conducted with the first applied voltage pulse in both a positive and negative polarity. In each situation, and for both sharp-to-sharp and sharp-to-flat electrode arrangements, we observe the discharge on the anode side. When the ICCD gate encompasses a positive applied voltage peak, along with a large EMI signal measured on the HPF-applied current trace, the corresponding image detects the glow on the HV side (Figure 10(a)). Likewise, when the electrode polarity is reversed in the sharp-to-sharp electrode configuration, using a voltage pulse with opposite polarity, the glow appears on the grounded anode electrode (Figure 10(b)). The EMI signal correlates with the side that the emission is detected in the bubble depending on the polarity of the applied voltage at a given measured event. In addition, the glow at the tip of a sharp electrode is sometimes observed at later times during secondary voltage oscillations. Figure 10(c) shows a later discharge event on the grounded electrode at which point the immediate voltage peak is negatively biased, and the grounded electrode is the anode in the configuration. Similarly, when the positive HV pulse is applied to the sharp electrode in the sharp-to-flat electrode configuration (Figure 7(b)), the discharge appears on the sharp electrode when it is of positive polarity. We do not see any light emission in this geometry when the applied pulse is negative. The glow at the tip of the positive electrode is the most persistent observation in all images where light is recorded.

D. Nanosecond Pulse Timescale: The Decay

In this section we report the results of observations made after the first half-wave of the initial applied voltage pulse, and discuss the behavior of the bubble/electrode system in the presence of the decaying pulse oscillations.

Multiple discharges are observed over the lifetime of the decaying signal initiating at alternating anodes. As depicted in Figure 10(b) and discussed in Section III C, a glow occurs on the grounded electrode during a negatively biased peak, provided a steep enough applied

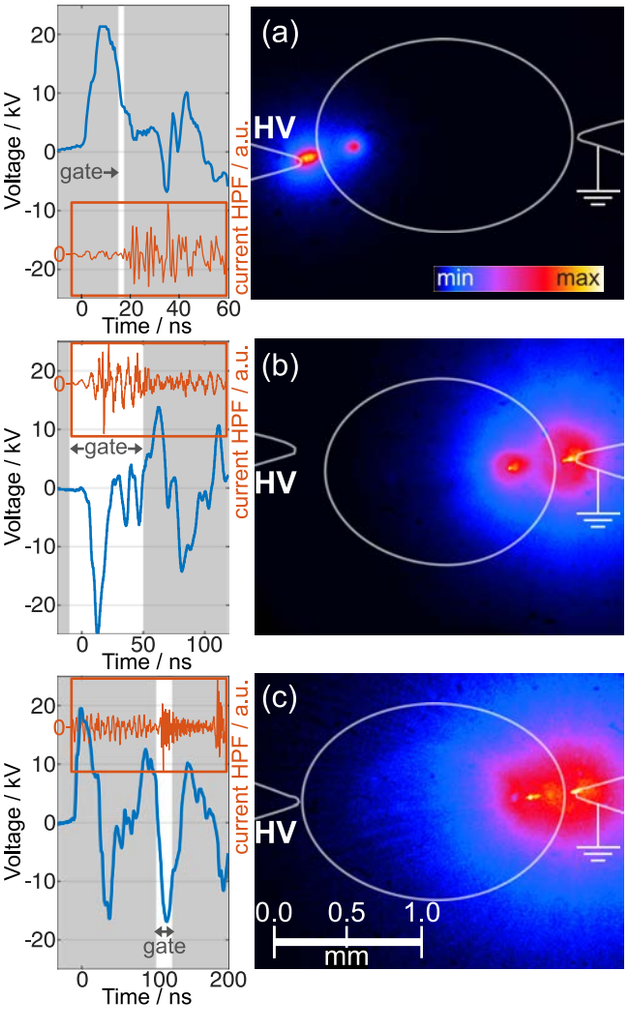

FIG. 10. Discharge initiation occurring at the anode. Emission is shown at (a) the HV electrode when the applied voltage is positive, and (b) the grounded electrode when the applied voltage pulse is negative. Delayed discharge occurs at the (c) grounded electrode when the corresponding applied voltage has reversed to negative polarity,thus, the anode. Image gate widths are (a) 5 ns, (b) 60 ns, and (c) 20 ns. Uncertainty for gate timing $\sigma_{\text{gate}} = 2\,\text{ns}$.

voltage rate of rise ($\mathrm{d}V/\mathrm{d}t$) is present. Likewise, later discharges have been observed to initiate multiple times throughout the decay of the voltage oscillations, on both electrodes when they swap anode arrangements (Figure 10(c)). The current traces associated with the images in Figure 11 show examples of multiple discharges occurring over hundreds of ns after the initial pulse. In the case of Figure 11(a), a negatively biased applied voltage results in the expected electrode-tip-to-bubble-apex breakdown at the grounded anode. The

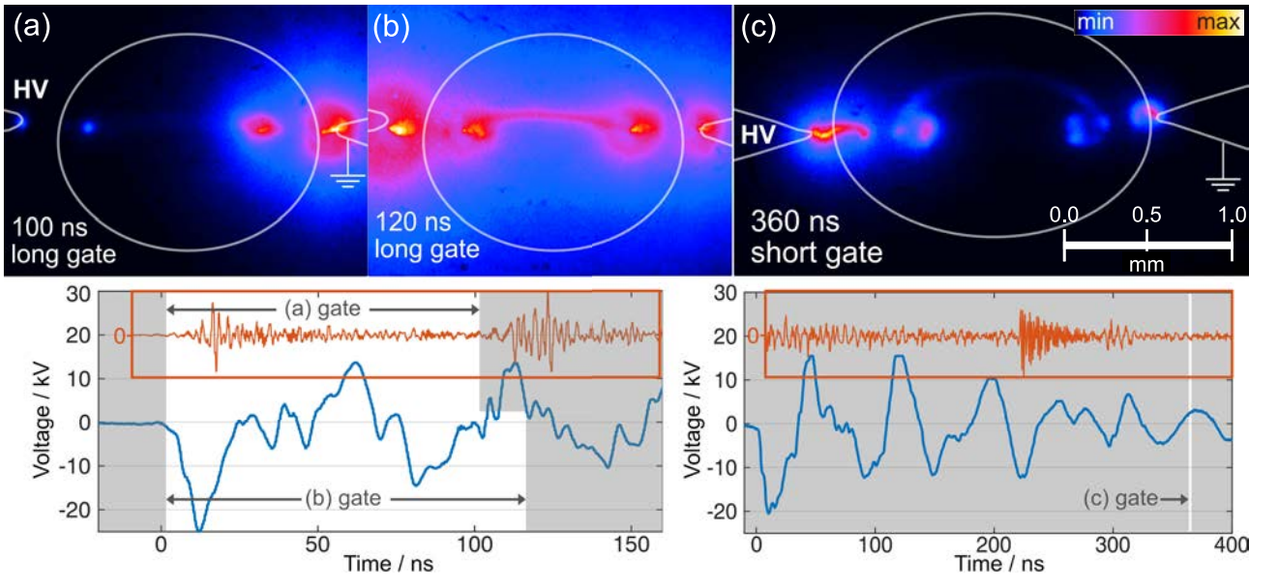

FIG. 11. Delayed discharges may occur throughout the decaying reflections of the initial HV pulse multiple times. Discharge initiated at the initial pulse (a) may appear to bridge the gas macrobubble due to later discharge from a reversed polarity anode (b). Short gate images taken at times much later than the last discharge show remnants of positions of previous discharges (c). Image gate width are (a) 100 ns, (b) 120 ns, and (c) 2 ns. Uncertainty for gate timing $\sigma_{\text{gate}} = 2\,\text{ns}$.

long gate-width, spanning both negative and positive applied voltage peaks, associated with this image also captures the characteristic tip glow on the HV electrode. However, over the course of 100 ns, the emission in the bubble is still limited to diffuse glow similar to the time regime covered in Section III B, emphasizing the lack of streamer formation. As discussed above, the ∼30 ns duration of the first half-wave is an insufficient amount of time to develop a streamer across the bubble, and this holds true for the subsequent reflected waves.

Figure 11(a & b) share remarkably similar applied voltage and current traces, but with slightly varying gate-widths. Detected emission that appears to bridge the bubble gap (Figure 11(b), Figure 4) can only be collected in the sharp-to-sharp electrode configuration where separate discharge initiations are allowed by alternating the anode from the HV electrode to the grounded electrode. The delay between the two images occurs at a positive applied voltage peak and at the initiation of a secondary discharge, as indication by the HPF current signal. As expected, a discharge on the positive voltage pulse is observed at the positive HV electrode. By comparing Figure 11(a & b) it is clear that the emission

detected between the 20 ns time difference facilitates excited regions of emission that are absent without the presence of breakdown on separate electrodes. This suggests that the emission observed in Figure 11(b), that spans the length of the bubble, is not the continuation of the initial discharge at the grounded electrode.

In addition, short gate-width images activated at times much later than the initial pulse can detect the history of the multiple discharges by observing decay from slower emission processes. Emission from electron-ion, ion-ion & dissociative recombination and Ar metastable excitation continues to produce photons well after the initial discharge. Argon optical emission can continue for several μs under low pressure and hundreds of ns at high pressure.[16,45] The oscilloscope trace for Figure 11(c) shows 2 discharge events as well as a 75 ns time range where high-frequency noise is higher in amplitude than normal. Distinct peaks from EMI noise suggest times where discharge events reach the argon bubble (∼25–100 ns, 220 ns, & 300 ns). The most noticeable of these signals occurs on a negative pulse 220 ns after the initial applied voltage rise-time begins and 140 ns before the opening of the ICCD gate. The corresponding image (short gate width of 2 ns) is open 80 ns after the last emission and retains visible evidence of these previous discharges. Though a single faint gap-bridging structure exists connecting a pair of emission spots within the bubble, the remaining spots are solitary.

Rough estimations for electron-ion recombination emission attenuation (approximating a characteristic decay time of ∼100 ns for atmospheric pressure) in Figure 11(c) are: 96–93% decrease for the initial noise across the first voltage period, 75% decrease for the large EMI event, and 45% decrease for the smaller EMI event. The initial emission intensity for each event is unknown, but the pattern presented across the bubble corresponds with multiple initiations on either side of the bubble over several hundreds of ns. This further emphasizes that long exposure images that capture multiple peaks are likely the collection of multiple discharge events initiated at consecutively alternating anode positions.

Finally, long-gate images are cross-referenced in the sharp-to-flat configuration. In the case where the sharp anode is held constant at one side of the bubble, the gap-extending emission captured in Figure 11(b) is absent. As expected, all of the EMI signals on the current HPF trace occur within a positive pulse. This means that the breakdown only occurs at a sharp electrode tip at times when it is the positive electrode. The lack of breakdown for negatively biased pulses is consistent throughout the sharp-to-flat images.

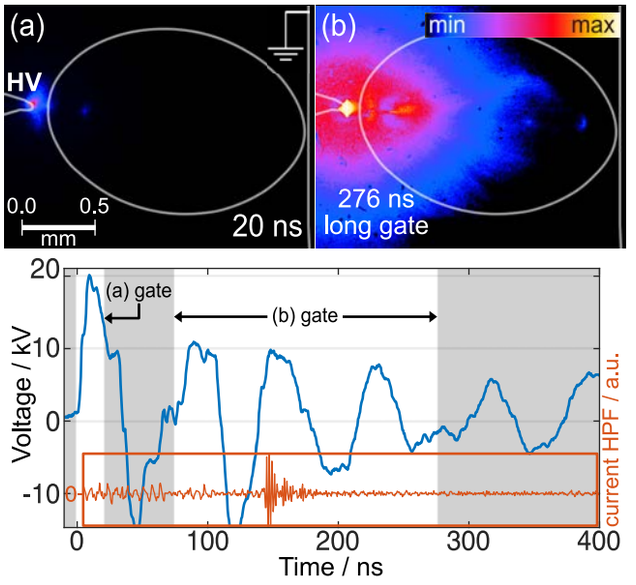

FIG. 12. Discharge at the HV electrode tip in which the (a) the gate begins at the applied voltage rise-time and (b) long exposure image initiated after 76 ns from the applied voltage rise-time in gas macrobubble for sharp-to-flat electrode configurations. The discharge event only appears in positive polarity pulse peaks. Image gate widths are (a) 20 ns and (b) 200 ns. Uncertainty for gate timing $\sigma_{\text{gate}} = 2\,\text{ns}$.

Figure 12 shows two images captured over the course of the applied voltage decay. The glow at the electrode tip begins around the peak of the initial pulse (Figure 12(a)); but in this case, the large EMI signal is not detected until the third positive pulse (Figure 12). To compare this electrode configuration with the sharp-to-sharp configuration from Figure 11, a long gate-width in the middle of the decaying applied voltage pulse is used. The gate collects light over 3 positive and negative peaks but does not show diffuse emission extending any further than what is observed for the first half-wave for the sharp-to-flat electrode configuration in Figure 9, suggesting that each spot is a new initiation over the course of the oscillating pulse decay.

To summarize all examples, emission detected spanning the gap of the bubble for oscillating ns pulses require anode breakdown to occur on both sides of the bubble. Despite breakdown on both sides, the emission observed with large gate-widths does not constitute proper streamer formation at our timescales (<500 ns). Instead, short gate-width images show the discharge being restrained to a diffuse Townsend mode and reoccur in this manner

over multiple events over the 500 ns oscillation decay.

IV. CONCLUSION

In this work we investigate the initiation of the discharge in the presence and absence of ∼1.7 mm Ar filled bubbles. Our primary observation is that the discharge is first observed at the sharp tip of a positive electrode, within the first 4–8 ns, with and without the Ar bubble present. The ANSYS Maxwell model shows that the presence of the Ar bubble effects the E-field in the region between the electrodes, but the field remains strong enough for the persistent presence of the glow at the submerged sharp positive electrode. The short rise-time of the applied voltage, and the time it takes for the discharge to bridge the gap between the tip of the sharp positive electrode and the apex of the bubble, suggest the electrostrictive cavitation mechanism for discharge initiation and propagation in water.

The discharge in the Ar bubble appears at times of 10–20 ns or within the first half-wave of the applied voltage. Since the falling voltage does not allow enough time to develop a streamer, the discharge appears to spread in a diffuse form remaining in the Townsend mode.

The same electrode tip and bubble behavior as observed during the first half-wave appears to repeat during some of the subsequent reflected pulses similarly at the sharp anode, which may occur at the opposite sharp electrode at different times. Images taken with long delays (>20 ns) show both electrodes and the bubble glowing, but the processes at the opposite electrodes appear during different voltage pulses and are visible together due to the emission decay times of hundreds of nanoseconds.

The experiment combines discharge in the water and discharge in a gas bubble on very fast time scales. The presented imaging study was possible due to an original optical timing system. The discharge behavior at these time scales is complex enough that estimates do not resolve the entire picture and detailed modeling is needed in order to understand the interactions and processes on this time scale.

ACKNOWLEDGMENTS

The work by NLS was supported by the Integrated University Program Graduate Fellowship. Work by KS was in part supported by the National Science Foundation under

Grant No. PHY 2107901. All plasma imaging was conducted at the Princeton Collaborative Research Facility (PCRF) which is supported by U.S. DOE under the contract No. DE-AC02-09CH11466. The work by SG was supported by PCRF. The authors thank Dr. M. Shneider for fruitful discussions.

AUTHOR DECLARATIONS

Conflict of Interest

The authors have no conflicts to disclose.

DATA AVAILABILITY STATEMENT

The data that support the findings of this study are available within the article [and its supplementary material]. Additional data that support the findings of this study are available from the corresponding author upon reasonable request.

REFERENCES

[1]R. Zhou, R. Zhou, K. Prasad, Z. Fang, R. Speight, K. Bazaka, and K. K. Ostrikov, "Cold atmospheric plasma activated water as a prospective disinfectant: the crucial role of peroxynitrite," Green Chemistry **20**, 5276–5284 (2018).

[2]M. Zhang, L. Qiu, and G. Liu, "Basic characteristics and application of micro-nano bubbles in water treatment," in *IOP Conference Series: Earth and Environmental Science*, Vol. 510 (IOP Publishing, 2020) p. 042050.

[3]H. Wang, Y. Wang, B. Wang, Y. Liu, and W. Zhang, "Surface microfabrication using coaxial waterjet assisted laser-induced plasma micromachining," Optics & Laser Technology **144**, 107446 (2021).

[4]P. J. Liew, J. Yan, and T. Kuriyagawa, "Fabrication of deep micro-holes in reaction-bonded sic by ultrasonic cavitation assisted micro-edm," International Journal of Machine Tools and Manufacture **76**, 13–20 (2014).

[5]S.-W. Kim, L. Peng, A. Miller, G. Beyer, E. Beyne, and C.-S. Lee, "Permanent wafer bonding in the low temperature by using various plasma enhanced chemical vapour deposi-

tion dielectrics," in *2015 International 3D Systems Integration Conference (3DIC)* (IEEE, 2015) pp. TS7–2.

[6]M. Shneider and M. Pekker, "Cavitation in dielectric fluid in inhomogeneous pulsed electric field," Journal of Applied Physics **114**, 214906 (2013).

[7]A. Ivanov, V. Nikiforov, S. Shevchenko, V. Y. Timoshenko, V. Pryadun, N. Bulychev, A. Bychenko, and M. Kazaryan, "Properties of metal oxide nanoparticles prepared by plasma discharge in water with ultrasonic cavitation," International Journal of Nanotechnology **14**, 618–626 (2017).

[8]J. Yang, H. C. Cramer III, and C. Franck, "Extracting non-linear viscoelastic material properties from violently-collapsing cavitation bubbles," Extreme Mechanics Letters **39**, 100839 (2020).

[9]Z. Shi, J. Wang, Z. Wang, Y. Qiao, T. Xiong, and Y. Zheng, "Cavitation erosion and jet impingement erosion behavior of the niti coating produced by air plasma spraying," Coatings **8**, 346 (2018).

[10]P. Zima, F. Maršík, and M. Sedlář, "Cavitation rates in water with dissolved gas and other impurities," Journal of Thermal Science **12**, 151–156 (2003).

[11]R. E. Apfel, "Role of impurities in cavitation threshold determination," The Journal of the Acoustical Society of America **46**, 93–93 (1969).

[12]M. N. Shneider and M. Pekker, *Liquid Dielectrics in an Inhomogeneous Pulsed Electric Field (Second Edition)*, 2053-2563 (IOP Publishing, 2019).

[13]P. Bruggeman, J. Degroote, J. Vierendeels, and C. Leys, "Dc-excited discharges in vapour bubbles in capillaries," Plasma Sources Science and Technology **17**, 025008 (2008).

[14]K. Tachibana, Y. Takekata, Y. Mizumoto, H. Motomura, and M. Jinno, "Analysis of a pulsed discharge within single bubbles in water under synchronized conditions," Plasma Sources Science and Technology **20**, 034005 (2011).

[15]S. Gershman, A. Belkind, and K. Becker, "Optical emission diagnostics of the plasma channel in a pulsed electrical discharge in a gas bubble," in *2009 IEEE Pulsed Power Conference* (IEEE, 2009) pp. 838–843.

[16]S. Gershman and A. Belkind, "Time-resolved processes in a pulsed electrical discharge in argon bubbles in water," The European Physical Journal D **60**, 661–672 (2010).

[17]B. S. Sommers, J. E. Foster, N. Y. Babaeva, and M. J. Kushner, "Observations of electric discharge streamer propagation and capillary oscillations on the surface of air bubbles in

water," Journal of Physics D: Applied Physics **44**, 082001 (2011).

[18]N. Y. Babaeva and M. J. Kushner, "Structure of positive streamers inside gaseous bubbles immersed in liquids," Journal of Physics D: Applied Physics **42**, 132003 (2009).

[19]W. Tian, K. Tachibana, and M. J. Kushner, "Plasmas sustained in bubbles in water: optical emission and excitation mechanisms," Journal of Physics D: Applied Physics **47**, 055202 (2013).

[20]B. Sommers and J. Foster, "Plasma formation in underwater gas bubbles," Plasma Sources Science and Technology **23**, 015020 (2014).

[21]K. Wang, S. I. Bhuiyan, M. A. H. Baky, J. Kraus, C. Campbell, X. Tang, H. Jemison, and D. Staack, "Role of bubble and impurity dynamics in electrical breakdown of dielectric liquids," Plasma Sources Science and Technology **30**, 055013 (2021).

[22]S. M. Korobeinikov, A. V. Melekhov, V. G. Posukh, V. M. Antonov, and M. Royak, "Experimental investigation of the behavior of bubbles in water under the effect of strong electric fields," High Temperature **39**, 163–168 (2001).

[23]S. M. Korobeinikov, A. V. Melekhov, and A. S. Besov, "Breakdown initiation in water with the aid of bubbles," High temperature **40**, 652–659 (2002).

[24]R. Joshi, J. Qian, G. Zhao, J. Kolb, K. Schoenbach, E. Schamiloglu, and J. Gaudet, "Are microbubbles necessary for the breakdown of liquid water subjected to a submicrosecond pulse?" Journal of Applied Physics **96**, 5129–5139 (2004).

[25]V. Panov, Y. M. Kulikov, E. Son, A. Tyuftyaev, M. K. Gadzhiev, and P. Akimov, "Electrical breakdown voltage of transformer oil with gas bubbles," High Temperature **52**, 770–773 (2014).

[26]Y. Hayashi, N. Takada, H. Kanda, and M. Goto, "Effect of fine bubbles on electric discharge in water," Plasma Sources Science and Technology **24**, 055023 (2015).

[27]N. Y. Babaeva, D. V. Tereshonok, and G. V. Naidis, "Initiation of breakdown in bubbles immersed in liquids: pre-existed charges versus bubble size," Journal of Physics D: Applied Physics **48**, 355201 (2015).

[28]M. Shneider, M. Pekker, and A. Fridman, "Theoretical study of the initial stage of sub-nanosecond pulsed breakdown in liquid dielectrics," IEEE Transactions on Dielectrics and Electrical Insulation **19**, 1579–1582 (2012).

[29]M. N. Shneider and M. Pekker, "Dielectric fluid in inhomogeneous pulsed electric field," Physical Review E **87**, 043004 (2013).

[30]D. Dobrynin, Y. Seepersad, M. Pekker, M. Shneider, G. Friedman, and A. Fridman, "Non-equilibrium nanosecond-pulsed plasma generation in the liquid phase (water, pdms) without bubbles: fast imaging, spectroscopy and leader-type model," Journal of Physics D: Applied Physics **46**, 105201 (2013).

[31]M. Šimek, P. Hoffer, J. Tungli, V. Prukner, J. Schmidt, P. Bílek, and Z. Bonaventura, "Investigation of the initial phases of nanosecond discharges in liquid water," Plasma Sources Science and Technology **29**, 064001 (2020).

[32]Z. Bonaventura, J. Tungli, P. Bílek, and M. Šimek, "Electron multiplication and avalanching in nanovoids at the initial stage of nanosecond discharge in liquid water," Plasma Sources Science and Technology **30**, 065023 (2021).

[33]D. Tereshonok, N. Y. Babaeva, G. Naidis, V. Panov, B. Smirnov, and E. Son, "Pre-breakdown phenomena and discharges in a gas-liquid system," Plasma Sources Science and Technology **27**, 045005 (2018).

[34]W. Graham and K. Stalder, "Plasmas in liquids and some of their applications in nanoscience," Journal of Physics D: Applied Physics **44**, 174037 (2011).

[35]A. Hamdan and M. S. Cha, "Ignition modes of nanosecond discharge with bubbles in distilled water," Journal of Physics D: Applied Physics **48**, 405206 (2015).

[36]N. Pillai, N. L. Sponsel, K. Stapelmann, and I. A. Bolotnov, "Direct numerical simulation of bubble formation through a submerged "flute" with experimental validation," Journal of Fluids Engineering **144** (2022).

[37]D. C. Smith, "Current probes, more useful than you think," in *1998 IEEE EMC Symposium. International Symposium on Electromagnetic Compatibility. Symposium Record (Cat. No. 98CH36253)*, Vol. 1 (IEEE, 1998) pp. 284–289.

[38]A. Sharma, K. Mishra, M. Raghuramaiah, P. Naik, and P. Gupta, "Design and performance characteristics of an electromagnetic interference shielded enclosure for high voltage pockels cell switching system," Sadhana **32**, 235–242 (2007).

[39]M. Pekker, Y. Seepersad, M. N. Shneider, A. Fridman, and D. Dobrynin, "Initiation stage of nanosecond breakdown in liquid," Journal of Physics D: Applied Physics **47**, 025502 (2013).

[40]K. Grosse, J. Held, M. Kai, and A. Von Keudell, "Nanosecond plasmas in water: ignition, cavitation and plasma parameters," Plasma Sources Science and Technology **28**, 085003 (2019).

[41]A. Von Keudell, K. Grosse, and V. Schulz-von der Gathen, "Nanosecond pulsed discharges in distilled water-part ii: line emission and plasma propagation," Plasma Sources Science and Technology **29**, 085021 (2020).

[42]X. Zhang and M. N. Shneider, "Electron generation and multiplication at the initial stage of nanosecond breakdown in water," Journal of Applied Physics **129**, 103302 (2021).

[43]P. Ceccato, O. Guaitella, M. R. Le Gloahec, and A. Rousseau, "Time-resolved nanosecond imaging of the propagation of a corona-like plasma discharge in water at positive applied voltage polarity," Journal of Physics D: Applied Physics **43**, 175202 (2010).

[44]Y. P. Raizer and J. E. Allen, *Gas discharge physics*, Vol. 1 (Springer, 1991).

[45]P. Bruggeman, T. Verreycken, M. A. Gonzalez, J. L. Walsh, M. G. Kong, C. Leys, and D. C. Schram, "Optical emission spectroscopy as a diagnostic for plasmas in liquids: opportunities and pitfalls," Journal of Physics D: Applied Physics **43**, 124005 (2010).

Journal of Vacuum Science Technology A

PLEASE CITE THIS ARTICLE AS DOI: 10.1116/6.0001990

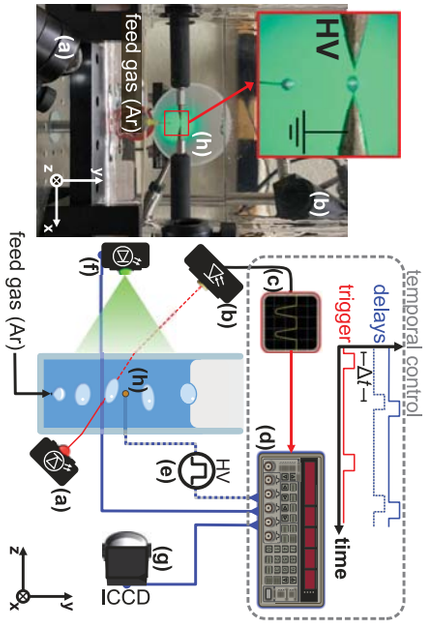

Journal of Vacuum Science Technology A

PLEASE CITE THIS ARTICLE AS DOI: 10.1116/6.0001990

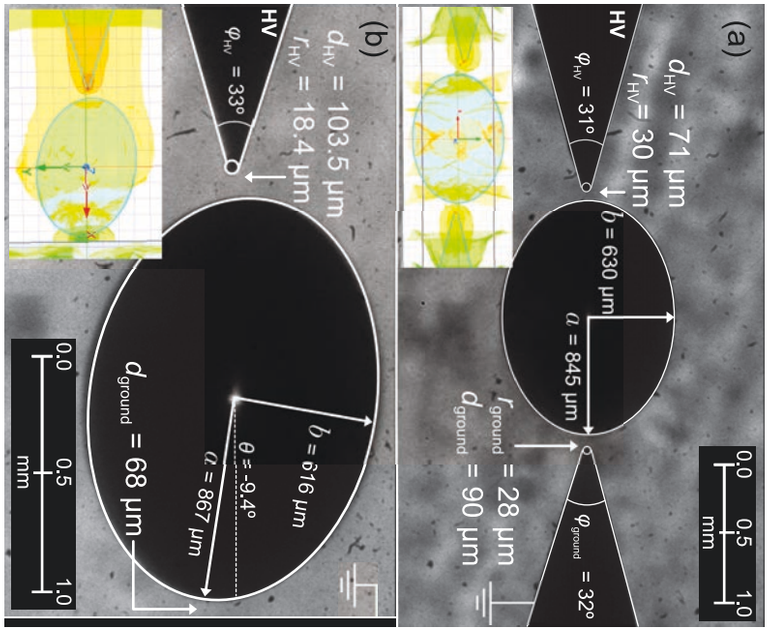

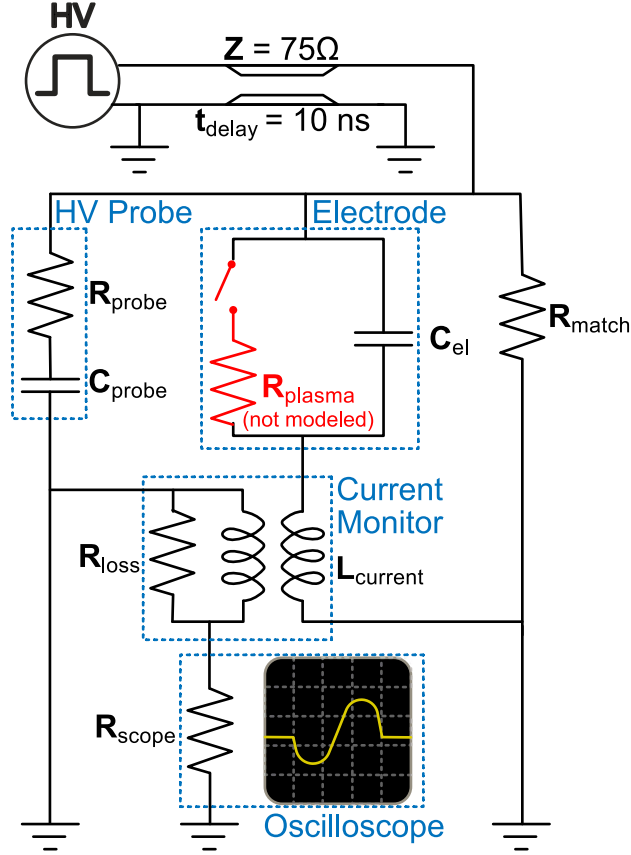

Journal of Vacuum Science Technology A

PLEASE CITE THIS ARTICLE AS DOI: 10.1116/6.0001990

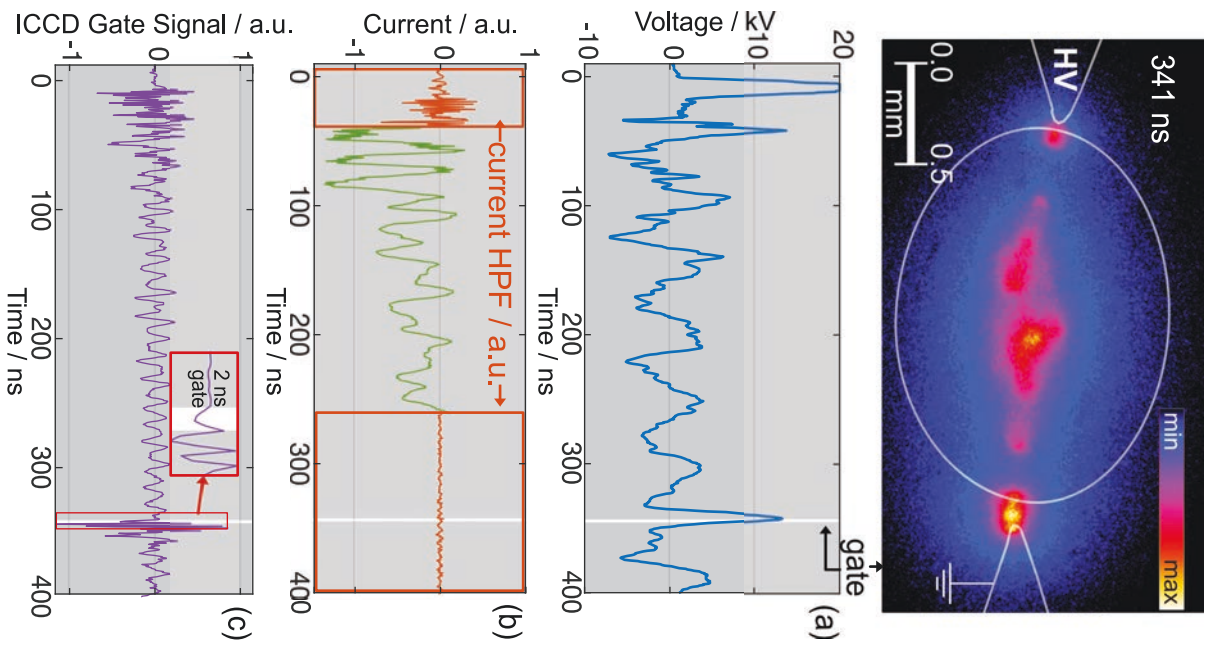

Journal of Vacuum Science Technology A

ACCEPTED MANUSCRIPT

This is the author's peer reviewed, accepted manuscript. However, the online version of record will be different from this version once it has been copyedited and typeset.
PLEASE CITE THIS ARTICLE AS DOI: 10.1116/6.0001990

Journal of Vacuum Science Technology A

ACCEPTED MANUSCRIPT

This is the author's peer reviewed, accepted manuscript. However, the online version of record will be different from this version once it has been copyedited and typeset.
PLEASE CITE THIS ARTICLE AS DOI: 10.1116/6.0001990

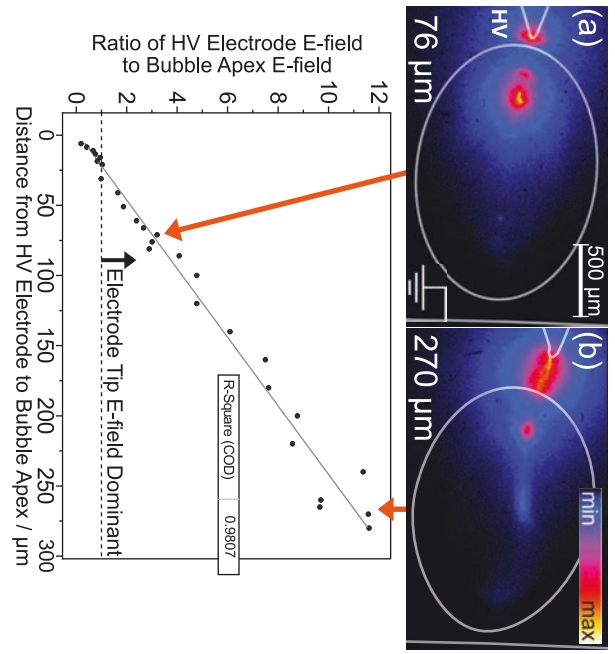

Journal of Vacuum Science Technology A

ACCEPTED MANUSCRIPT

This is the author's peer reviewed, accepted manuscript. However, the online version of record will be different from this version once it has been copyedited and typeset.
PLEASE CITE THIS ARTICLE AS DOI: 10.1116/6.0001990

Journal of Vacuum Science Technology A

ACCEPTED MANUSCRIPT

This is the author's peer reviewed, accepted manuscript. However, the online version of record will be different from this version once it has been copyedited and typeset.
PLEASE CITE THIS ARTICLE AS DOI: 10.1116/6.0001990

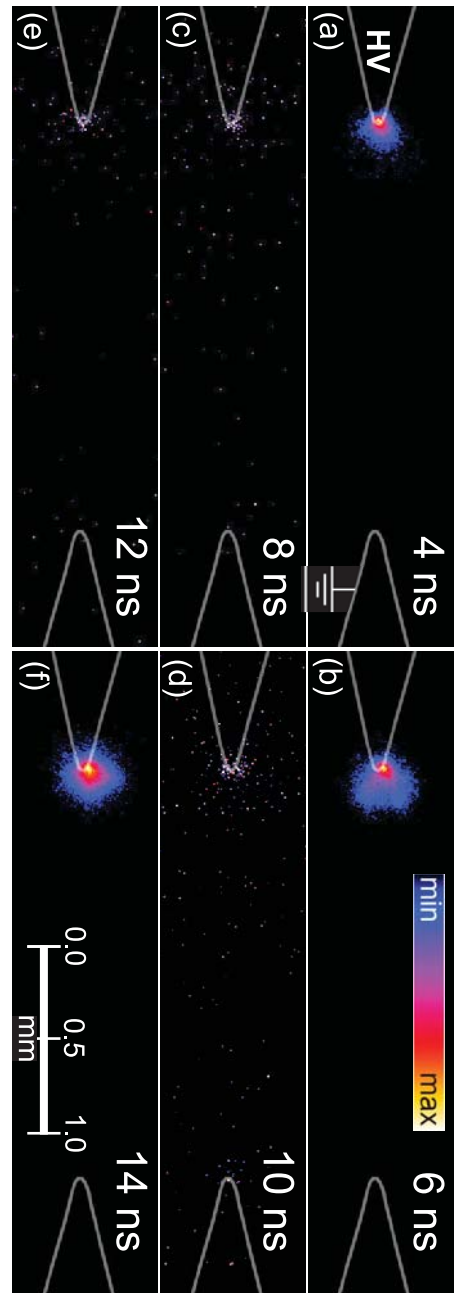

Journal of Vacuum Science Technology A

ACCEPTED MANUSCRIPT

This is the author's peer reviewed, accepted manuscript. However, the online version of record will be different from this version once it has been copyedited and typeset.
PLEASE CITE THIS ARTICLE AS DOI: 10.1116/6.0001990

Journal of Vacuum Science Technology A

ACCEPTED MANUSCRIPT

This is the author's peer reviewed, accepted manuscript. However, the online version of record will be different from this version once it has been copyedited and typeset.
PLEASE CITE THIS ARTICLE AS DOI: 10.1116/6.0001990

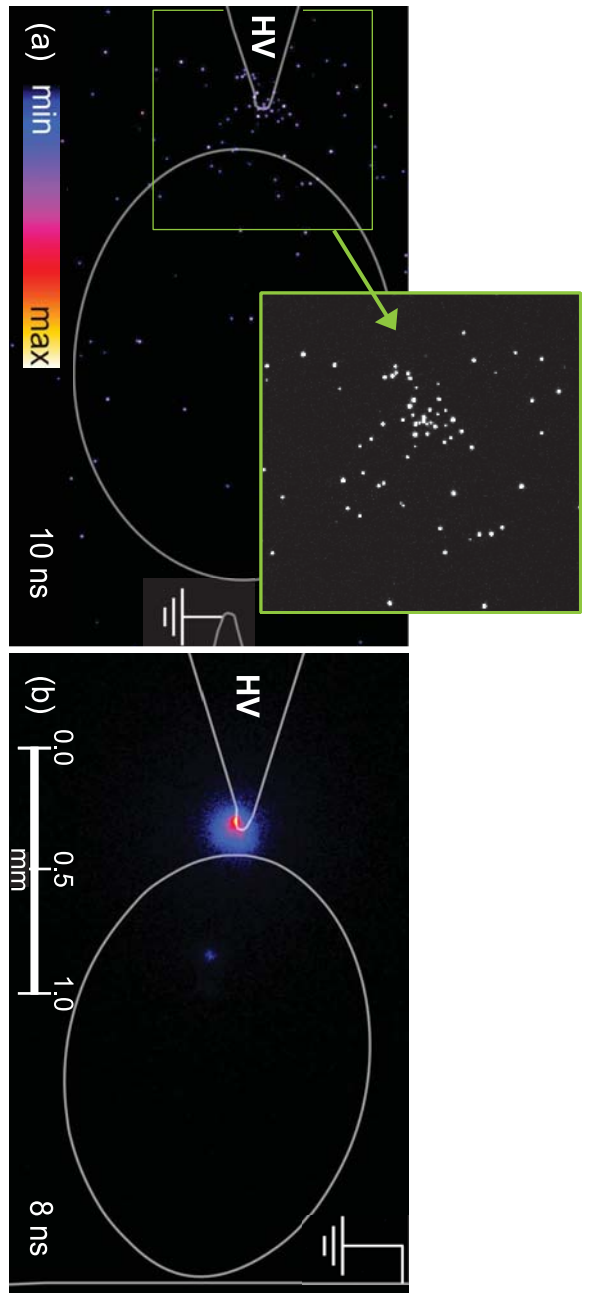

Journal of Vacuum Science Technology A

ACCEPTED MANUSCRIPT

This is the author's peer reviewed, accepted manuscript. However, the online version of record will be different from this version once it has been copyedited and typeset.
PLEASE CITE THIS ARTICLE AS DOI: 10.1116/6.0001990

Journal of Vacuum Science Technology A

PLEASE CITE THIS ARTICLE AS DOI: 10.1116/6.0001990

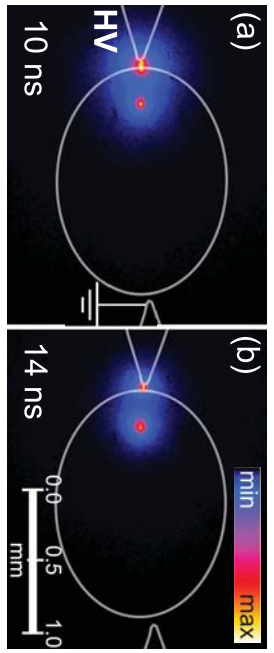

Journal of Vacuum Science Technology A

ACCEPTED MANUSCRIPT

This is the author's peer reviewed, accepted manuscript. However, the online version of record will be different from this version once it has been copyedited and typeset.
PLEASE CITE THIS ARTICLE AS DOI: 10.1116/6.0001990

Journal of Vacuum Science Technology A

ACCEPTED MANUSCRIPT

This is the author's peer reviewed, accepted manuscript. However, the online version of record will be different from this version once it has been copyedited and typeset.
PLEASE CITE THIS ARTICLE AS DOI: 10.1116/6.0001990

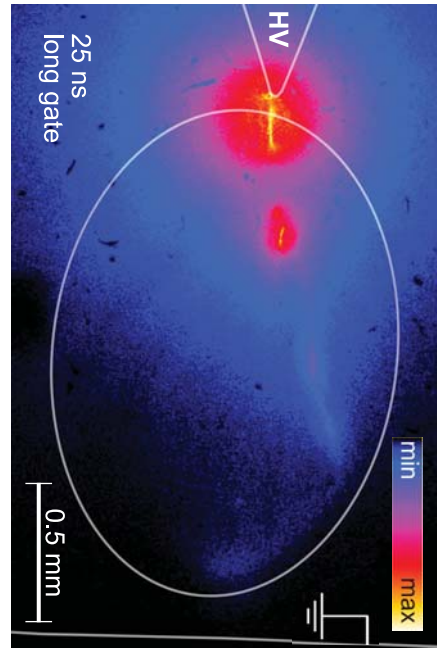

Journal of Vacuum Science Technology A

ACCEPTED MANUSCRIPT

This is the author's peer reviewed, accepted manuscript. However, the online version of record will be different from this version once it has been copyedited and typeset.
PLEASE CITE THIS ARTICLE AS DOI: 10.1116/6.0001990

Journal of Vacuum Science Technology A

ACCEPTED MANUSCRIPT

This is the author's peer reviewed, accepted manuscript. However, the online version of record will be different from this version once it has been copyedited and typeset.
PLEASE CITE THIS ARTICLE AS DOI: 10.1116/6.0001990

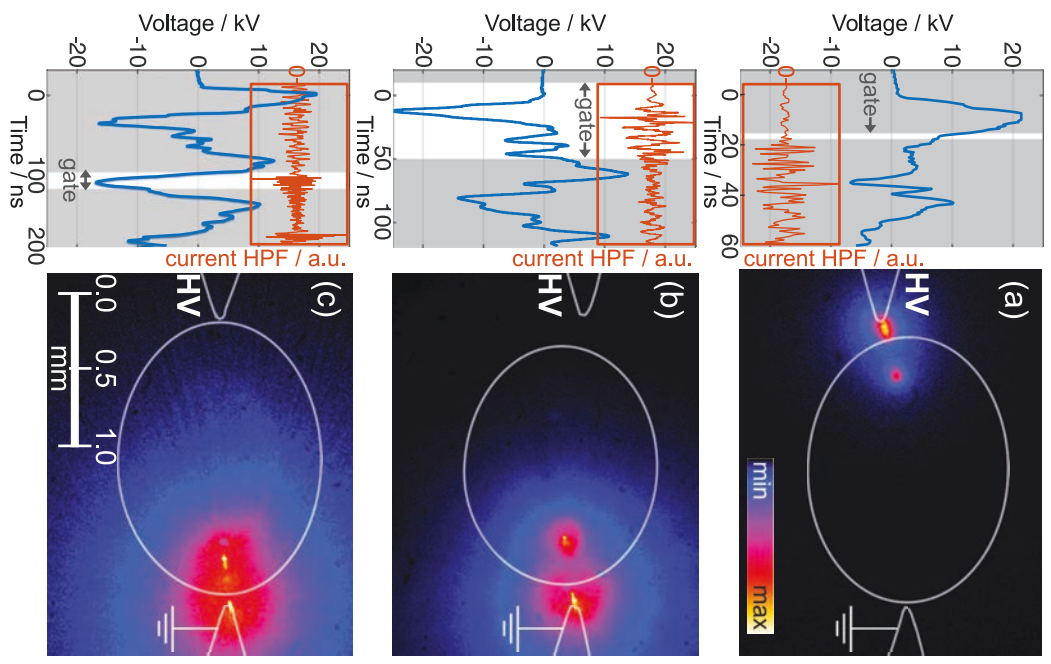

Journal of Vacuum Science Technology A

ACCEPTED MANUSCRIPT

This is the author's peer reviewed, accepted manuscript. However, the online version of record will be different from this version once it has been copyedited and typeset.
PLEASE CITE THIS ARTICLE AS DOI: 10.1116/6.0001990

Journal of Vacuum Science Technology A

ACCEPTED MANUSCRIPT

This is the author's peer reviewed, accepted manuscript. However, the online version of record will be different from this version once it has been copyedited and typeset.
PLEASE CITE THIS ARTICLE AS DOI: 10.1116/6.0001990

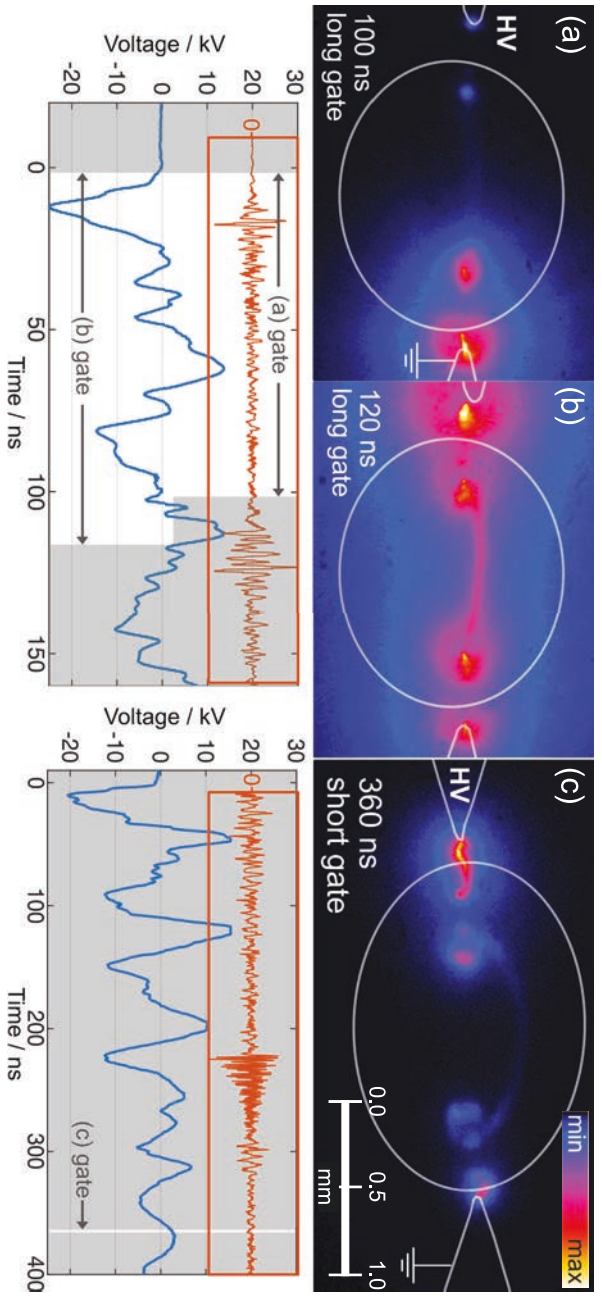

Journal of Vacuum Science Technology A

ACCEPTED MANUSCRIPT

This is the author's peer reviewed, accepted manuscript. However, the online version of record will be different from this version once it has been copyedited and typeset.
PLEASE CITE THIS ARTICLE AS DOI: 10.1116/6.0001990

Journal of Vacuum Science Technology A

ACCEPTED MANUSCRIPT

This is the author's peer reviewed, accepted manuscript. However, the online version of record will be different from this version once it has been copyedited and typeset.
PLEASE CITE THIS ARTICLE AS DOI: 10.1116/6.0001990

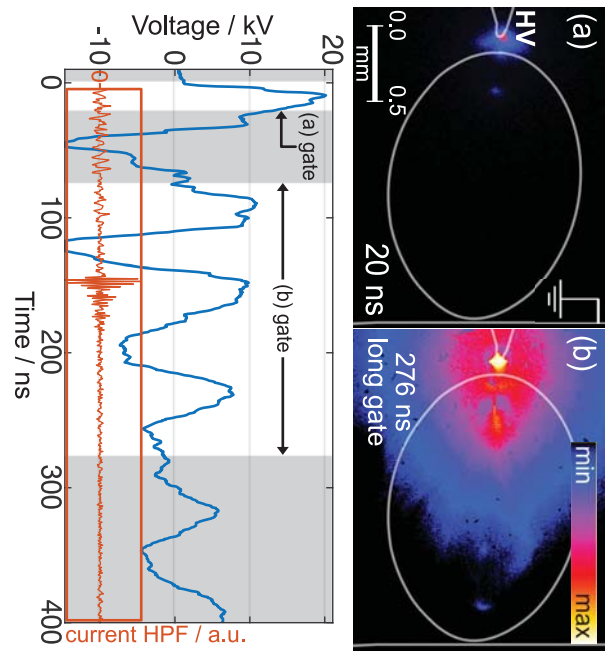

Journal of Vacuum Science Technology A

ACCEPTED MANUSCRIPT

This is the author's peer reviewed, accepted manuscript. However, the online version of record will be different from this version once it has been copyedited and typeset.
PLEASE CITE THIS ARTICLE AS DOI: 10.1116/6.0001990